

The EUMETSAT
Network of
Satellite
Application
Facilities



O3M SAF

Ozone and Atmospheric
Chemistry Monitoring

ALGORITHM THEORETICAL BASIS DOCUMENT

NRT and Offline Vertical Ozone Profile and Tropospheric Ozone Column Products

Prepared by:

Roeland van Oss, Johan de
Haan, Olaf Tuinder (KNMI)
with contributions from Andy
Delcloo (KMI)

Royal Netherlands Meteorological Institute

DOCUMENT STATUS SHEET

Issue	Date	Modified Items / Reason for Change
0.1	2006-11-14	First draft version
0.2	2007-06-06	Revised after ORR-A2 comments
0.3	2007-08-30	Revised after ORR-A2 review
0.4	2007-10-30	Revised based on open RIDs
0.5	2008-03-12	More revisions based on open RIDs
0.6	2008-04-18	Revised based on ORRA-3 RID
0.7	2008-09-30	Revisions for ORR-B Most references to GOME-1 hidden. Chapter 7: Error analysis updated.
0.8	2009-09-01	QualityInput check on cloud top pressure vs surface pressure. Level1b input and usage revised (section 5.2).
1.0	2010-04-29	Update of logos. Description of CEA0 fitting.
1.01	2010-05-25	Added info on O3MSAF
1.10	2011-11-16	Added section on Tropospheric Ozone Column (TrOC). Chapter / section headers of ozone profile made specific. Added sentences to TrOC in generic profile sections.
1.11	2012-02-20	Update of description of TrOC and StrOC calculation. Added plots from Delcloo (RMI) on TrOC. Added TrOC error analysis section.
1.12	2012-03-19	Revised based on ORR/PCR RIDs
1.13	2012-05-11	Revised based on outcome of ORR (2012-03-20)
1.14	2013-05-28	Updated SAA filter. Updated slit function. Introduction of second GOME-2 instrument (Metop-A and Metop-B)
1.15	2013-06-16	Changes based on ORR RIDs. Acronyms added. <i>A priori</i> harmonisation
1.16	2014-11-12	Section Scope and Heritage were adapted to indicate the origins of the algorithm and source of the software more clearly.
1.17	2015-02-09	Relates to Software version 1.32, Algorithm version 1.12, OPF version 3.20. Update of the calculation method of the tropospheric vertical integrated ozone profile (tropospheric ozone column) in Chapter 10.
1.30	2015-07-01	Changes based on RIDs from the TrO3 review.

TABLE OF CONTENTS

1. INTRODUCTION.....	6
1.1 Purpose	6
1.2 Scope	6
1.3 Heritage.....	6
1.4 Glossary.....	6
1.4.1 Acronyms.....	6
2. INTRODUCTION TO EUMETSAT SATELLITE APPLICATION FACILITY ON OZONE AND ATMOSPHERIC CHEMISTRY MONITORING (O3M SAF)	8
2.1 Background.....	8
2.2 Objectives	8
2.3 Product families.....	8
2.4 Product timeliness and dissemination.....	9
2.5 Information	9
3. OVERVIEW.....	10
4. OZONE PROFILE RETRIEVAL ALGORITHM BACKGROUND	11
4.1 The need for satellite ozone profile measurements	11
4.2 Ozone profile retrieval from nadir UV earthshine spectra	11
4.2.1 SBUV	12
4.2.2 ERS-2 and GOME-1	13
4.2.3 MetOp and GOME-2	15
4.2.3.1 MetOp.....	15
4.2.3.2 GOME-2.....	15
4.2.4 SCIAMACHY and OMI.....	16
5. OZONE PROFILE RETRIEVAL ALGORITHM DESCRIPTION	18
5.1 Overview	18
5.1.1 Data flow	18
5.1.2 Control Flow	20
5.2 The forward model.....	21
5.2.1 Introduction	21
5.2.2 Atmospheric state input to the RTM.....	21
5.2.2.1 Trace Gas Databases	21
5.2.2.2 Aerosols	22
5.2.2.3 Temperature, pressure and altitude	22
5.2.2.4 Clouds	23

5.2.2.5	Surface albedo	23
5.2.3	Radiative transfer model (RTM)	23
5.2.3.1	Single-scattering RTM	23
5.2.3.2	Multiple-scattering RTM	23
5.2.3.3	Computation of Jacobians	25
5.2.3.4	Sphericity correction at large viewing angle	25
5.2.3.5	Polarisation Correction	26
5.2.3.6	Raman scattering	27
5.2.3.7	Computing the instrument radiance measurement	30
5.3	Inversion using Optimal Estimation	31
6.	IMPLEMENTATION OF THE OPERATIONAL OZONE PROFILE RETRIEVAL ALGORITHM	34
6.1	Retrieval and model grid	34
6.2	Level 1 Input and usage	34
6.2.1	Level 1b	34
6.2.2	South Atlantic Anomaly	35
6.2.3	Additive Offset	36
6.3	Level 2 output of the vertical ozone profile retrieval	36
6.4	Definition of the state vector and <i>a priori</i>	37
6.5	Performance Considerations	37
6.5.1	Forward Model Efficiency	37
6.5.2	Fitting Window	40
7.	VERTICAL OZONE PROFILE INFORMATION	42
7.1	Averaging kernels	42
8.	EVALUATION OF THE ACCURACY OF THE OZONE PROFILE USING ERROR ANALYSIS	46
8.1	Test data set: Input configuration	47
8.2	Error analysis results	47
9.	VERTICAL OZONE PROFILE VALIDATION	52
10.	PARTIAL INTEGRATION OF VERTICAL OZONE PROFILES	55
10.1	General	55
10.1.1	Calculation of partial ozone columns and its associated error	55
10.1.2	Tropopause definitions	56
10.1.3	Examples: the tropospheric and stratospheric columns	57
10.2	Error sensitivity of the Tropospheric ozone column	58
11.	REFERENCES	65

1. INTRODUCTION

1.1 Purpose

This document is the Algorithm Theoretical Baseline Document for OPERA: the Ozone Profile Retrieval Algorithm and derived quantities for GOME based on Optimal Estimation. This document presents the scientific background of the algorithm, presents an outline of its implementation and provides a clear understanding of the ozone profile data product. For those parts of the algorithm where different alternatives exist, the choices made are clarified. The document also presents an error analysis, including an analysis of the product quality under special circumstances.

1.2 Scope

This ATBD provides information on OPERA: the optimal-estimation retrieval algorithm used to derive ozone profiles from the GOME level-1b product.

1.3 Heritage

This algorithm, and the software implementing it, was developed within the framework of the ESA projects CHEOPS-GOME and the Ozone Climate Change Initiative (O3-CCI), and the EUMETSAT projects GOME-2-Tools, UVN-Tools and the Satellite Application Facility on Ozone and Atmospheric Chemistry Monitoring (O3M SAF).

The document also explains how the Tropospheric and Stratospheric Ozone Columns are derived from the profile.

1.4 Glossary

1.4.1 Acronyms

ATBD	Algorithm Theoretical Basis Document
B&P	Bass and Paur
DAK	Doubling-Adding KNMI
DFS	Degrees of Freedom for Signal
ECMWF	European Centre for Medium-range Weather Forecast
ERS	European Remote Sensing Satellite
ESA	European Space Agency
EUMETSAT	European Organisation for the Exploitation of Meteorological Satellites

FRESCO	Fast Retrieval Scheme for Cloud Observables
FWHM	Full Width Half Maximum
GDP	GOME Data Processor
GOME	Global Ozone Monitoring Instrument
KNMI	Royal Netherlands Meteorological Institute
LIDORT	Linearized Discrete Ordinate Radiative Transfer
LUT	Look Up Table
NHP	NRT High resolution ozone Profile
NOP	NRT Ozone Profile (in coarse resolution)
NTO	NRT Total Ozone
O3MSAF	Satellite Application Facility on Ozone Monitoring
OE	Optimal Estimation
OHP	Offline High resolution ozone Profile
OMI	Ozone Monitoring Instrument
OOP	Offline Ozone Profile (in coarse resolution)
OPERA	Ozone Profile Retrieval Algorithm
PMD	Polarization Measurement Device
PSC	Polar Stratospheric Clouds
RMS	Root Mean Square
RTM	Radiative Transfer Model
SAF	Satellite Application Facility
SAGE	Stratospheric Aerosol and Gas Experiment
SBUV	Solar Backscatter Ultra-Violet radiometer
StrOC	Stratospheric Ozone Column
SW	Software
SZA	Solar Zenith Angle
TOMS	Total Ozone Mapping Spectrometer
TrOC	Tropospheric Ozone Column
UV	Ultra Violet
VIS	Visible

2. INTRODUCTION TO EUMETSAT SATELLITE APPLICATION FACILITY ON OZONE AND ATMOSPHERIC CHEMISTRY MONITORING (O3M SAF)

2.1 Background

The need for atmospheric chemistry monitoring was first realized when severe loss of stratospheric ozone was detected over the Polar Regions. At the same time, increased levels of ultraviolet radiation were observed.

Ultraviolet radiation is known to be dangerous to humans and animals (causing e.g. skin cancer, cataract, immune suppression) and having harmful effects on agriculture, forests and oceanic food chain. In addition, the global warming - besides affecting the atmospheric chemistry - also enhances the ozone depletion by cooling the stratosphere. Combined, these phenomena have immense effects on the whole planet. Therefore, monitoring the chemical composition of the atmosphere is a very important duty for EUMETSAT and the world-wide scientific community.

2.2 Objectives

The main objectives of the O3M SAF is to process, archive, validate and disseminate atmospheric composition products (O₃, NO₂, SO₂, OCIO, HCHO, BrO, H₂O), aerosols and surface ultraviolet radiation utilising the satellites of EUMETSAT. The majority of the O3M SAF products are based on data from the GOME-2 spectrometer onboard MetOp-A satellite.

Another important task of the O3M SAF is the research and development in radiative transfer modelling and inversion methods for obtaining long-term, high-quality atmospheric composition products from the satellite measurements.

2.3 Product families

Near real-time Total Column (NTO)

O₃, NO₂, O₃Tropo, NO₂Tropo

Near real-time Ozone Profile (NOP)

Near real-time UV Index (NUV)

Offline Total Column (OTO)

O3, NO2, O3Tropo, NO2Tropo, SO2, BrO, H2O, HCHO, OCIO

Offline Ozone Profile (OOP)

Offline Surface UV (OUV)

Aerosols (ARS)

2.4 Product timeliness and dissemination

Data products are divided in two categories depending on how quickly they are available to users:

Near real-time products are available in less than three hours after measurement. These products are disseminated via EUMETCast (NOP, NHP, NTO), GTS (NOP, NHP, NTO) or Internet (NUV).

Offline products are available in two weeks from the measurement and they are archived at the O3M SAF archives in Finnish Meteorological Institute (OOP, OHP, OUV, ARS) and German Aerospace Center (OTO).

Only products with “pre-operational” or “operational” status are disseminated. Up-to-date status of the products and ordering info is available on the O3M SAF website.

2.5 Information

Information about the O3M SAF project, products and services:
<http://o3msaf.fmi.fi/>

O3M SAF Helpdesk: o3msaf@fmi.fi

3. OVERVIEW

The algorithm OPERA retrieves the information on the vertical distribution of ozone contained in a GOME UV Earthshine spectrum. It operates by finding the ozone profile that gives a best match between the measured and a simulated spectrum. The latter is computed by radiative transfer computation. The retrieval is ill-posed in the sense that many profiles give similar simulated spectra within given error bars. This is treated by using Optimal Estimation for the selection of the solution. Optimal Estimation employs *a priori* information to select the optimal solution.

In the following sections we describe the ozone profile retrieval algorithm in more detail. In particular the radiative transfer model and the inversion method are discussed. Also, an error analysis will be provided.

Derived from the vertical ozone profile the Tropospheric and Stratospheric Ozone Columns can be derived. This is described in the last sections of this document.

4. OZONE PROFILE RETRIEVAL ALGORITHM BACKGROUND

4.1 The need for satellite ozone profile measurements

There is a great need for information on the global three-dimensional distribution of ozone in the atmosphere. Time series of ozone spanning years or even decades are important to detect changes in ozone that are coupled to climate change and to monitor and understand the depletion and expected recovery of stratospheric ozone. Stratospheric ozone measurements are used for operational numerical weather prediction models to constrain the energy balance in the stratosphere and allow improved forecasts. Fast availability of the measurements is crucial for this use. Knowledge on the distribution of ozone in the upper troposphere is important to quantify its contribution to radiation forcing and thus improve understanding of climate change. Ozone in the boundary layer has adverse health effects and is one of the key species in air quality. Ozone is formed in the atmosphere from gases like nitrogen (di)oxide and hydrocarbons. These ozone precursors are emitted by traffic, industry and biomass burning. The detection of air pollution from space offers the possibility to follow the long-range transport of air pollutants, complementing surface measurements and modelling.

Ozone profiles measured by earth observing satellite instruments offer the required day-to-day and global picture that is needed to bring the scientific understanding of climate change and air pollution forward. If prolonged for decades the ozone satellite data will provide invaluable information on the changing atmosphere.

4.2 Ozone profile retrieval from nadir UV earthshine spectra

The development of ozone profile retrieval methods from space-born measurements has started with the ozone profile retrieval from UV ground measurements with the Umkehr technique. *Singer & Wentworth* [1957] were the first to realize that, by using artificial satellites that measure the backscattered solar UV radiation emerging from the Earth atmosphere, information on the vertical distribution of ozone can be obtained. They proposed to use observations at different solar angles. *Twomey* [1961] made an important step towards a practical method by showing how to retrieve the ozone profile from a single earthshine spectrum. The method solves an inverse problem: the ozone profile determines the spectrum, but the spectrum is measured and the ozone profile is to be retrieved from it. Information on the vertical distribution of ozone is contained in the earth radiance measured from space in the wavelength range between about 260 to 340 nm. This is due to the strongly varying ozone absorption cross section in this range. It varies from a maximum of 0.3 DU^{-1} at 260 nm to 0.01 DU^{-1} at 300 nm to 0.001 DU^{-1} at 315 nm, see Figure 1.

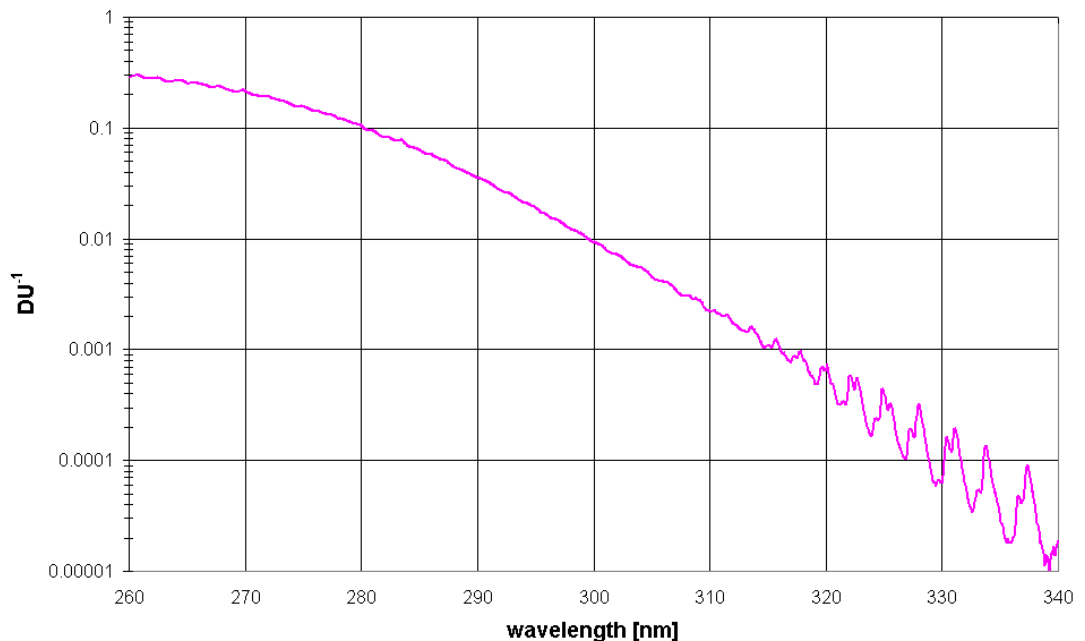


Figure 1: Ozone cross sections in inverse Dobson Units for a temperature of 200 K.

Considering that a typical total ozone column varies between 150 and 500 DU, the atmosphere varies from almost completely opaque to transparent in this wavelength interval. At 260 nm only scattering from the top layer of the atmosphere containing a few DU of ozone contributes to the back-scattered radiance since the solar light does not penetrate any deeper. Moving to longer wavelengths, deeper layers start to contribute to the back-scattered radiance. Between 300–310 nm a sizeable fraction of the solar light reaches the surface, depending on the solar zenith angle. The combination of earthshine radiances in the spectral range [260–310 nm] therefore yields information on the column-amount of scattering agents (mainly air molecules) as a function of ozone column, counted from the top. Since the column density of air molecules above a pressure level is proportional to the pressure, due to hydrostatic equilibrium, the ozone profile information in the spectrum is primarily the functional relation of pressure and ozone column density. Scattering by aerosol, extinction by molecular scattering and multiple scattering complicates this simple picture somewhat, but it captures the essence of the ozone profile retrieval.

4.2.1 SBUV

An operational ozone profile retrieval algorithm has been developed for the BUUV, SBUV, SBUV/2 and SSBUV experiments [Bhartia *et al.* 1996, and references therein). The algorithm retrieves ozone profile information from nadir radiance measurements at 12 wavelengths between 255 and 340 nm. The algorithm calculates a profile as 12 partial columns between 13 fixed pressure levels. These levels are at $(\frac{1}{2})^n \times 1013.25$ mbar, with $n = 0, 2, 3, \dots, 12$. The top level is zero pressure. The profile is also given as ozone mixing ratios at 19 pressure

levels, obtained from the first derivative of a cubic spline of $X(P)$ with 12 nodes. These nodes are the pressure levels described above without the top (zero) level.

The SBUV algorithm performs an inversion of the single scattering approximation to extract the ozone profile from the measured radiances. For the shortest wavelengths (< 297 nm) the single scattering approximation is a good approximation for the radiance. At longer wavelengths the radiance is enhanced with an amount I_{msr} due to reflectance at the surface and multiple scattering. The algorithm subtracts this term from the measured radiance before performing the inversion. Look-up tables have been pre-computed and are used to calculate I_{msr} , given the total ozone, the surface pressure, the so-called Lambert-equivalent reflectivity (LER) and the solar zenith angle. The first three quantities are derived from the longest wavelength (339.8 nm) using calculated radiances for a model atmosphere without aerosols and a Lambertian reflecting ground surface. The derived value for LER then incorporates the effect of aerosols and non-Lambertian ground reflectance.

The final retrieval is performed using an iterative employment of Optimal Estimation [Rogers, 1976, 1990]. The SBUV profiles are valid for the range [1–20 mbar], with RMS errors ranging from 5–15 %. Outside this range the dependence on *a priori* information is too large and only the partial columns outside this range are useful.

4.2.2 ERS-2 and GOME-1

The Global Ozone Monitoring Experiment (GOME-1) on board the ESA ERS2 satellite [Burrows *et al.*, 1999] improves on SBUV for the retrieval of ozone profiles due to its better spectral coverage and resolution. GOME measures the earthshine spectrum continuously between 240 and 790 nm, with a resolution ranging from 0.17 to 0.3 nm. GOME scans the earth atmosphere using a scan mirror, which rotates perpendicular to the flight direction (approximately North-South) from 31 degrees to -31 degrees in 4.5 seconds (forward scan) and back in 1.5 seconds (backwards scan). Each 1.5 seconds the detectors are read out. Nominally, the scan mirror covers a swath of about 960 km, so during the forward scan spectra of three ground pixels of 320 km are measured. The size of the ground pixel in the flight direction is governed by the slit opening and amounts to 40 km. For the smallest wavelengths the signal-to-noise ratio is too small for the 1.5 seconds integration. Therefore part of Band 1, Band 1a, is read-out every 12 seconds, corresponding to a ground pixel of 960 x 80 km. The upper wavelength of Band 1a is set at the start of mission to 307 nm, but in June 1998 it is shifted to 287 nm. To correct for its polarization sensitivity, GOME measures the degree of polarization using three dedicated Polarization Measurement Devices (PMDs) covering the spectral ranges 300-400, 400-600, and 600-800 nm, respectively. As the PMDs are read out much faster, every 93,75 ms, than the spectral channels, they also have higher horizontal resolution. Every nominal pixel covers 16 PMD pixels. This subpixel information is used to determine the cloud fraction making them useful for cloud detection purposes. GOME spectra, i.e., geolocated, spectrally and radiometrically calibrated solar irradiances and earthshine radiances, have been supplied by ESA through the GOME Data Processor (GDP)

[DLR, 1996]. The calibration includes a correction for the polarization sensitivity, which has an additional option to correct the spectra for polarization effects.

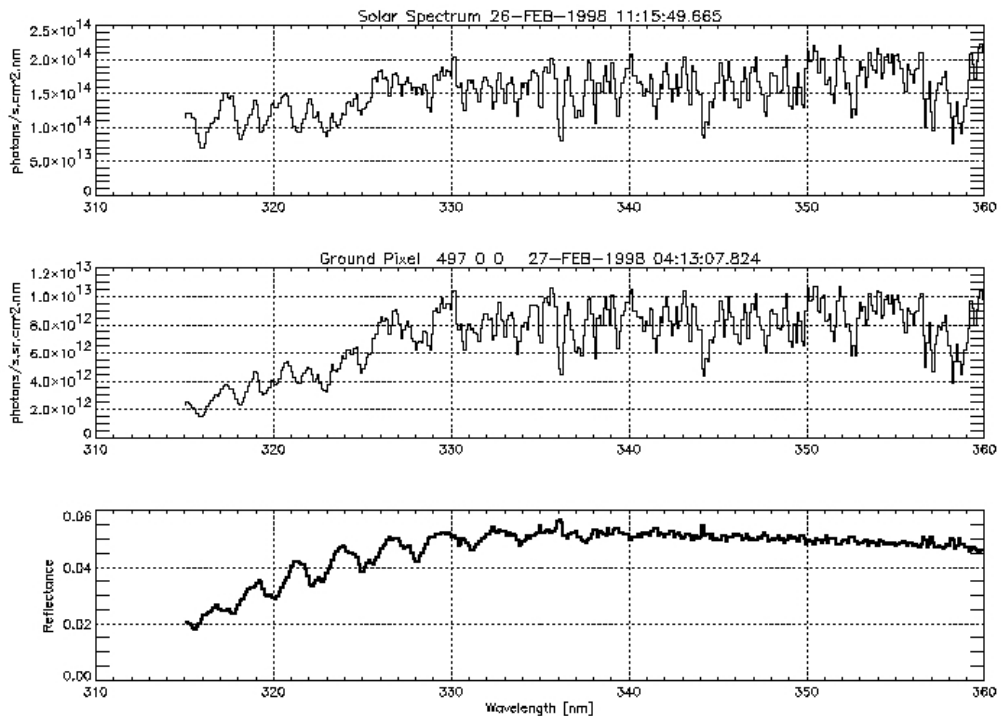


Figure 2: Example of an earthshine spectrum, a solar spectrum and their ratio, the reflectance measured by GOME on 26 February 1998. Only part of Band 2 is shown containing the Huggins absorption band of ozone (the oscillating structures in the reflectance between 315 and 340 nm).

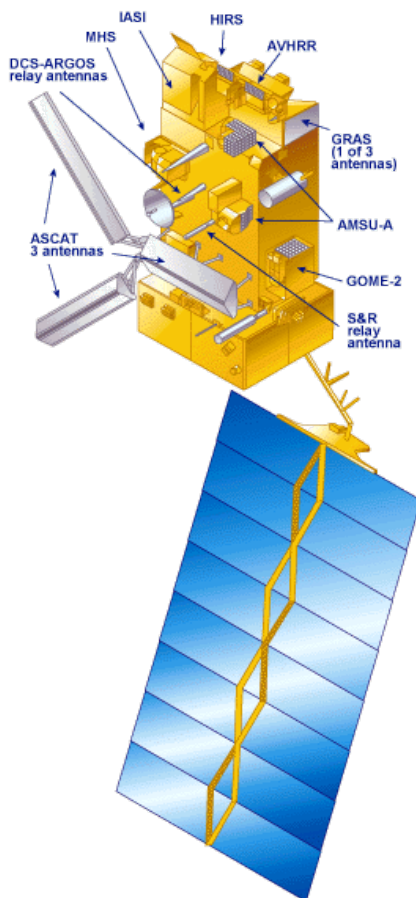
Once per day the solar irradiance spectrum is measured which is used to compute the atmospheric reflectance, or sun-normalized radiance.

Ozone profile-retrieval algorithms for GOME have been developed by *Munro et al.* [1998], *Hoogen et al.* [1999], *Van der A et al.* [1998] and *Van Oss & Spurr* [2000], *Hasekamp & Landgraf* [2001], *Müller et al.* [2003].

Munro et al. [1998], *Hoogen et al.* [1999] use on-line radiative transfer modeling with the GOMETRAN model [*Roazanov et al.*, 1997, 1998] and optimal estimation for the inversion. *Van Oss & Spurr* [2002] use the LIDORT model [*Spurr et al.*, 2000; *Van Oss & Spurr*, 2002] and also optimal estimation. *Hasekamp & Landgraf* [2001] use a different inversion method (Phillips-Tikhonov) and an RTM (LIRA) that deals with polarization [*Hasekamp et al.*, 2002]. A different kind of ozone profile algorithm, not based on forward modeling and inversion, but utilizing neural network techniques has been developed by *Müller et al.* [2003]. The different retrieval methods have been inter-compared in conjunction with ground based measurements in a study by the “ozone profile working group” e.g.: by *Meijer et al* [2006].

4.2.3 MetOp and GOME-2

4.2.3.1 MetOp



The MetOp satellite series is the core element of the EUMETSAT Polar System (EPS), developed in partnership with the European Space Agency. It carries a complement of new European instruments, as well as versions of operational instruments flown on the corresponding NOAA satellites of the USA.

The EUMETSAT programme includes provision for the development of the MetOp spacecraft in conjunction with the European Space Agency (ESA), the construction and launch of three new MetOp spacecraft, the development of the corresponding instruments and ground infrastructure, and provision for routine operations over a period of 15 years from the date of first launch. This polar system is complementary to EUMETSAT's existing Meteosat satellites in geostationary orbit.

The two EPS MetOp satellites (MetOp-A and MetOp-B) fly in a sun-synchronous polar orbit at an altitude of about 840 km, circling the planet 14 times each day and crossing the equator at 09:30 local (sun) time on each descending (south-bound) orbit. Successive orbits are displaced westward due to the Earth's own rotation, giving global coverage of

most parameters at least twice each day, once in daylight and once at night.

The spacecraft carries a comprehensive set of instrumentation, designed primarily to support operational meteorology and climate monitoring, but also supporting many additional applications.

4.2.3.2 GOME-2



METOP carries a number of instruments including the Global Ozone Monitoring Experiment-2 (GOME-2). This instrument is designed to measure the total column and profiles of atmospheric ozone and the distribution of other key atmospheric constituents. GOME-2 is a nadir viewing

across-track scanning spectrometer with a swath width of 1920 km. It measures the radiance back-scattered from the atmosphere and the surface of the Earth in the ultraviolet and visible range. The instrument uses four channels to cover the full spectral range from 200 to 790 nm with a spectral sampling of 0.11 nm at the lower end of the range, rising to 0.22 nm at the higher end. The instrument employs a mirror mechanism which scans across the satellite track with a maximum scan angle that can be varied from ground control, and three multi-spectral samples per scan. The ground pixel size of GOME-2 is 80 x 40 km² for the shortest integration times, but is usually 8 times larger for the detector measuring the shortest UV wavelengths.

Table 1; GOME-2 properties (for MetOp-A)

Spectrometer type	double spectrometer with pre-disperser prism and four holographic gratings
Spectral range	240 –790 nm
Field of view	0.286° (across track) x 2.75° (along track)
Entrance slit	0.2 mm (across track) x 9.6 mm (along track)
Channels (Bands) & sampling & resolution	1a: 203 – 306 nm & 0.14 - 0.11 nm & 0.24 – 0.29 nm 1b: 306 – 322 nm & +/- 0.11 nm & 0.24 – 0.29 nm 2a: 290 – 399 nm & +/- 0.13 nm & 0.26 – 0.28 nm 2b: 299 – 412 nm & +/- 0.13 nm & 0.26 – 0.28 nm 3: 391 – 607 nm & +/- 0.22 nm & 0.44 – 0.53 nm 4: 584 – 798 nm & +/- 0.22 nm & 0.44 – 0.53 nm
Polarisation monitoring unit	250 detector pixels 312 – 790 nm in 12 programmable bands spectral resolution: 2.8 nm at 312 nm to 40 nm at 790 nm
Swath widths	1920 km (nominal mode), 960 km, 320 km, 240 km, 120 km
Solar calibration	Once per day
Spectral calibration	fixed angle (once per day to once per month)
White Light Source Dark signal	fixed angle (night side of the orbit)
Default spatial resolution and integration time	Band 1a: 640 km x 40 km (1920 km swath and integration time of 1.5 s) Band 1b – 4: 80 km x 40 km (1920 km swath and int. time of 0.1875 s) PMD: 10 km x 40 km (for polarisation monitoring)

4.2.4 SCIAMACHY and OMI

The experience with GOME-1 has proven to be very useful for the specification and preparation of two successors of GOME: SCIAMACHY on ENVISAT (launched March 2002) and OMI on EOS-AURA (launched July 2004). These two space-born spectrometers all measure the UV wavelength range from nadir (SCIAMACHY also in limb and occultation) that is needed to retrieve information on the vertical distribution of ozone.

The KNMI ozone profile software, called Opera, is developed to be applicable to all four instruments. Also for OMI KNMI has the responsibility to prepare an ozone profile retrieval algorithm.

5. OZONE PROFILE RETRIEVAL ALGORITHM DESCRIPTION

5.1 Overview

The ozone profile algorithm (Opera) derives from selected spectral windows in the earthshine measurement a best estimate of the ozone profile. The earthshine spectrum is simulated by applying a radiative transfer model (RTM). Input to the RTM are viewing and solar angles, surface albedo, cloud properties and trace gas (including ozone) and aerosol profiles. A set of parameters (state vector) including the ozone profile is iteratively adjusted, followed by recomputation of the earthshine spectrum until the measured and simulated spectra agree satisfying certain convergence criteria. Figure 3 shows the flow diagram of Opera. Below the function of the main modules and data structures are shortly described.

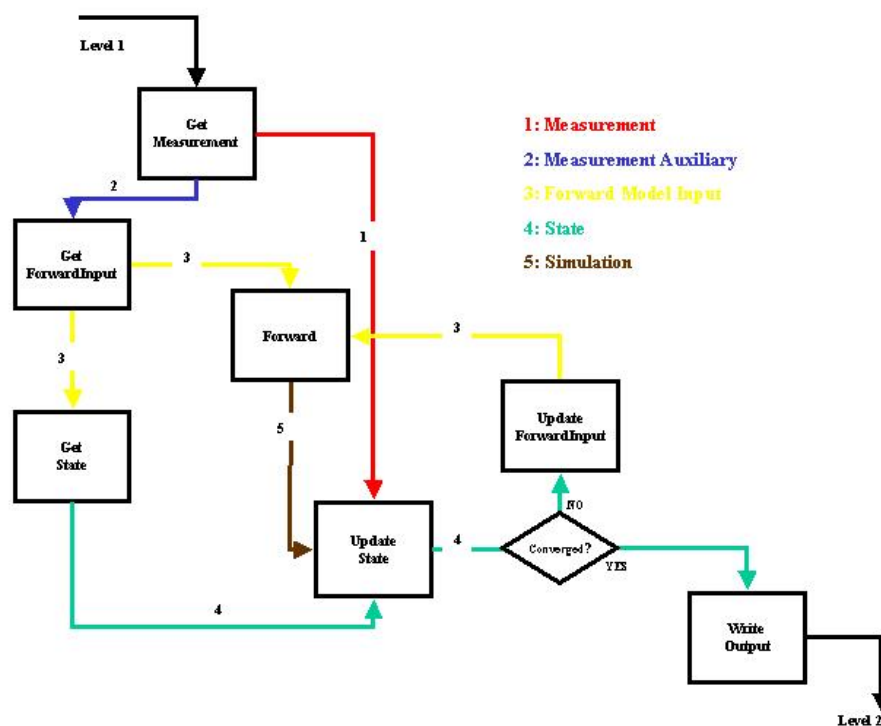


Figure 3: Main modules and data structures of Opera.

5.1.1 Data flow

Input to Opera is GOME-2 binary EPS Level 1b data (PFS version 12). The use of the Level 1 input is further outlined in Section 6.2.

Output of Opera is the Level 2 ozone profile output file, containing the retrieved ozone profile and all information on the retrieval that is important to use and interpret the product. The output product is discussed in Section 6.3 and completely described in the Product User Manual (PUM) of the O3MSAF offline and near real time ozone profiles..

The main data structures of Opera are:

1. Measurement

This data structure contains the set of spectral measurements extracted from the level 1b data and used to retrieve ozone profile information from

2. Measurement Auxiliary

This data structure contains the auxiliary data of the spectral measurement that is needed to simulate the measurements, like solar and viewing angles, geolocation, time and date. Some parameters are derived from level 1b parameters, like terrain height and cloud parameters

3. Forward Model Input

This data structure includes the complete set of parameters that are needed to simulate the measurement: altitude, pressure, temperature, aerosol and trace gas profiles, viewing and solar angles, surface albedo, cloud parameters.

4. State

This data structure contains the set of parameters that are retrieved from the measurements. It contains the ozone partial columns for all layers and auxiliary parameters, specified by the user of the software. The structure also includes the *a priori* and the error covariance matrices.

5. Simulation

This data structure includes a part that has the same form as measurement, only it contains the simulated measurement and it contains the weighting functions.

Not included in this list are the subroutine that read the user supplied configuration file and subroutines to read reference data, such as climatologies and cross sections.

The main modules of Opera are:

- Get Measurement

The Level 1 file is read and the set of spectral measurements to be used for retrieval and the auxiliary data are extracted from it.

- Get Forward Model Input

Based on the level 1 auxiliary data the Forward Model Input data structure is build.

- Get State

Given user input on what to retrieve, the state vector (initial value and a *priori*) are extracted from Forward Model Input

- Forward

The forward model simulates the measurement and the derivatives of all elements of the measurement with respect to all state elements (weighting functions), given Forward Model Input. The forward model includes a radiative transfer model that simulates the radiance entering the instrument and an instrument model that computes the actual radiance as contained in the level 1 product.

- Update State

This is the inversion model; it is run to produce a best estimate of the state vector using the simulation, the weighting functions and the measurement.

- Update Forward Model Input

Given the updated state vector, the corresponding elements of Forward Model Input are updated for the next simulation.

- Write Output

The output product, including the retrieved ozone profile, is written to file.

5.1.2 Control Flow

After the State update, convergence is checked given inverse model diagnostics. If convergence has been reached the output is written, otherwise the program loops back to update the Forward Model Input and to Forward for a next iteration step. A maximum number of iterations is pre-set and checked. If it is exceeded the retrieval has failed and the output of the current state is saved.

After the output has been saved, the program loops back to Get Measurement to check if there are more retrievals are to be performed. If so the next measurements is extracted from level 1 and the next retrieval starts. If not, the program ends with writing all saved data to output file.

Below we outline the two main modules (Forward and Update State (Inversion)) and provide arguments for specific choices.

5.2 The forward model

5.2.1 Introduction

The forward model consists of a radiative transfer model (RTM) that computes the radiances at the entrance of the instrument, and a slit function convolution that simulates the level 1 radiance values. The RTM has two parts. The single-scattering component and its Jacobian are computed separately using high vertical resolution ozone profiles. The multiple scattering component is computed at lower vertical resolution using the radiative transfer model LIDORTA.

In the following we describe the atmospheric set-up for the RTM, followed by a description of the single scattering RTM and the LIDORTA RTM. In this section we also deal with accuracy and optimisation aspects of the RTM. In the last section we describe the Instrument Model.

5.2.2 Atmospheric state input to the RTM

For input, the RTM requires the following: a pressure grid, atmospheric profiles and cross-sections of trace gases (ozone and interfering species such as NO₂ and SO₂), aerosol profiles and optical parameters, surface reflection parameters, cloud parameters, solar and viewing polar and azimuth angles, the wavelength grid and the solar irradiance at these wavelengths. The vertical grid is based on user input, but default it consists of 40 layers between 41 fixed pressure levels: from 1000 to 0.1 hPa, where the levels in between have a fixed ratio. The actual surface pressure replaces the nominal 1000 hPa level. For cloudy and partially cloudy scenes, the cloud-top pressure replaces the nearest pressure level.

5.2.2.1 Trace Gas Databases

For ozone distributions, the source of the global ozone climatology can be user selected via the configuration file. This climatology will be used as *a priori* and as initial profile if no better information is available. In normal operations, usually one of the possible climatologies will be selected, so that a consistent dataset becomes available.

The climatologies available to Opera are from:

- *Fortuin & Kelder* [1999]: which provides ozone-mixing ratios at 19 pressure levels for each month at 17 latitude bands. It also provides full error statistics.
 - TOMS version 8 climatology: this climatology is more recent and supposedly more accurate than Fortuin & Kelder. Given month, latitude band and the total ozone column, then a profile in terms of layer partial columns can be extracted. Because the total ozone column is input for the TOMS v8 selection, a dedicated total ozone algorithm or pre-computed total ozone values would be required. Currently, the Opera software uses the relatively simple TIDAS method [Zehner [2005]] to get a first guess total ozone column from two selected radiances and an air mass factor. Although TIDAS is good as a first guess, a DOAS retrieval method would often be better validated and used in a wide range of situations.
-

- *McPeters et al* [2006]: mixing ratios at 18 latitude bands and 61 vertical pressure levels for each month of the year, based on 15 years of ozone sonde measurements (1988-2002) and SAGE (v6.1) and UARS/MLS data. The actual choice of the *a priori* and initial ozone climatology will be made after a validation study. The name of the climatology selected is written in the output product for user to refer to.

With regards to the ozone cross sections used in Opera, one has a choice of using a temperature-parameterised data set of *Bass & Paur* [1985], corrected according to *Chance* [2001] and *Orphal* [2001], or a temperature parameterised cross section data set made from work by *Daumont et al* [1992], *Malicet et al* [1995] and *Brion et al* [1993]. For NO₂ and SO₂, we take an initial distribution profile from the AFGL data set [*Anderson et al.*, 1986]. NO₂ cross-sections are taken from the reference data set of *Vandaele* [1998], SO₂ cross section from the HITRAN molecular database [*Rothman et al.*, 1992]. For Rayleigh cross sections and depolarisation values, empirical formulae are used based from *Bates* [1984]. The actual choice of the cross section database is saved as a parameter in the output product. Please refer to the Product User Manual for more details on where to find this information in the level-2 product.

5.2.2.2 Aerosols

The LOWTRAN 7 [*Berk et al.*, 1989] database of aerosol models is used in the forward model. Database vertical profiles of aerosol optical properties (extinction, scattering, absorption, single scattering albedo and asymmetry parameter from *Deepak et al*, 1983) are interpolated to the RTM pressure and wavelength grids. The aerosol regime is selected based on surface type (land or ocean), season and lower atmosphere humidity profile for the boundary layer and troposphere. For higher layers the LOWTRAN stratospheric background is taken.

5.2.2.3 Temperature, pressure and altitude

The temperature profile is required for the determination of ozone cross sections, which, in turn, are used to calculate layer optical thickness values. In hydrostatic equilibrium, the pressure difference can be related directly to the column number density of air. For historical measurements, the ERA-40 data set can be used up to the year 2000. After 2000, analyses or 6-12 hour forecast of global fields from the ECMWF operational model can be used. The ECMWF temperature data needs a pre-processing step to convert them into a format that Opera can read. The surface pressure is also obtained from the ERA-40 or operational ECMWF data, and is needed to calculate the pressure levels of the original ECMWF model.

In the case of GOME-2, the ground height comes from the Level 1b data. Hydrostatic equilibrium is used to compute the altitude grid from pressure and temperature.

When no temperature data set is available for the location and date, then the software will revert to a temperature climatology, based on zonally averaged, monthly mean temperature values from ECMWF.

5.2.2.4 Clouds

Cloud properties such as cloud top pressure, cloud fraction and cloud albedo are used in the forward model. The GOME-2 Level 1b product contains pre-computed cloud values which are calculated with an improved FRESCO algorithm (*Wang and Stammes* [2007]). The treatment of clouds in the forward model assumes a Lambertian reflective surface at cloud top for the cloudy fraction of the pixel. The FRESCO algorithm assumes a fixed cloud-top albedo of 80% at the wavelength region of the O2 A-band. If the clouded fraction dominates the observed radiance (cloud fraction > 15%) the cloud top albedo is retrieved and the surface albedo fixed. We assume that cloudy and clear parts of a pixel do not exhibit significant 3-D radiative transport effects and thus are treated independently. The model level that is nearest to the cloud pressure is replaced by the latter.

5.2.2.5 Surface albedo

For the surface reflectance condition, the baseline RTM treatment assumes a Lambertian reflecting surface. Only if the clouded fraction does not dominate the observed radiance (cloud fraction < 15%) the surface albedo is retrieved and the cloud albedo fixed.

5.2.3 Radiative transfer model (RTM)

Given the atmospheric profiles and the cross sections, a set of optical parameters is defined for each layer; this set constitutes the basic input to the radiative transfer model for a single wavelength. These optical parameters are: layer optical thickness and single scattering albedo, and a sufficient number of phase function expansion coefficients and the exact phase function evaluated at the scattering angle for the single scattering contribution. The RTM further requires the solar irradiance at each wavelength to compute the earth radiance. The radiative transfer problem is solved using separate models for the single and multiple scattered components.

5.2.3.1 Single-scattering RTM

The single-scattered radiance at TOA and the associated Jacobian is computed using an analytic solution that includes the attenuation due to the spherical shell atmosphere along the photon path [*van Oss & Spurr*, 2002]. The phase function is specified to high accuracy by using its exact value at the scattering angle. This procedure is similar to the Nakajima-Tanaka correction [*Nakajima & Tanaka*, 1988], included in the latest DISORT version (version 2).

5.2.3.2 Multiple-scattering RTM

The LIDORTA [*van Oss & Spurr*, 2002] discrete-ordinate RTM is used for the multiple scattering computations. In an atmosphere divided into a number of optically uniform adjacent layers, the radiative transfer equation (RTE) is first solved for each layer; this is followed by the application of boundary conditions to match the radiation field at layer interfaces. The atmosphere is illuminated by a downward-directed parallel beam of sunlight. The diffuse radiation (excluding the

attenuated direct solar beam) is solved for the whole atmosphere. Atmospheric sphericity effects on the direct beam attenuation are treated with the pseudo-spherical "average secant" approximation [Caudill *et al.*, 1997, Spurr, 2001]. Polarisation is not considered in the RTE solution. A separate look-up table, described in section 5.2.3.5, is used to correct for this neglect.

For a given wavelength λ we define for each layer p (where $p = 1, \dots, P$): ω_p , the single scattering albedo (ratio of the total scattering and extinction coefficients); $\Delta\tau_p = \tau_p - \tau_{p-1}$, the layer optical thickness for total extinction. τ is the vertical coordinate; τ is zero at the top of the atmosphere. Each atmospheric layer is further characterised by a set of phase function Legendre moments $\beta_{l,p}$. The RTE for unpolarised diffuse light is:

$$\begin{aligned} \mu \frac{dI(\mu, \phi, \tau)}{d\tau} &= I(\mu, \phi, \tau) - J(\mu, \phi, \tau) \\ J(\mu, \phi, \tau) &= \frac{\omega}{4\pi} \iint P_s(\mu, \phi, \mu', \phi') I(\mu', \phi') d\mu' d\phi' + \\ &\quad \frac{\omega}{4\pi} P_s(\mu, \phi, -\mu_0, \phi_0) I_0 \exp(-\sigma\tau) \end{aligned} \quad (1.)$$

where μ is the cosine of the polar angle, ϕ is the azimuth angle and P_s is the phase function for scattering. The source function J comprises the scattered diffuse radiation (first term) and the primary scattering (second term). The direct solar beam has extra-terrestrial irradiance I_0 , polar direction $-\mu_0$ and azimuth ϕ_0 . The factor σ in the exponential is the average secant multiplier that accounts for the attenuation of the solar light in a spherical-shell geometry.

Eq. (1.) is solved by first expanding the diffuse intensity field and the phase functions in a Fourier series in the cosine of the relative azimuth angle $\phi - \phi_0$, and then by approximating the polar angle integration of the diffuse scatter term with a summation using a double-Gauss quadrature scheme [Chandrasekhar, 1960]. We use N to denote the number of half-space streams in the summation. For one Fourier term in the general case, the resulting set of coupled linear differential equations is usually solved using standard numerical packages [Stamnes *et al.*, 1988]. For $N=2$ and $N=3$ (the 4-and 6-stream cases), the RTE solutions can be written down directly without recourse to numerical tools [van Oss & Spurr, 2002]. Solutions for all layers are combined using a set of boundary conditions: (a) continuity of the radiance field at layer interfaces, (b) no down-welling diffuse light at TOA, and (c) a Lambertian reflectance condition at the bottom of the atmosphere (BOA). The resulting linear system for the unknown integration constants is solved with the help of special band-matrix LU-decomposition routines from the LAPACK suite [Anderson *et al.*, 1995]. This completes the discrete ordinate solution at quadrature directions and at every optical depth in the atmosphere. To derive the radiance at TOA at an arbitrary viewing direction (θ, ϕ) , we substitute the discrete ordinate solution at the quadrature streams in the multiple scatter integrals in the original RTE, and integrate the latter. The result is:

$$I(0, \mu, \phi) = I_{surf}(\tau_p, \mu, \phi) e^{-\tau_p/\mu} + \sum_{p=1}^P \Lambda_p(\mu, \phi) e^{-\tau_{p-1}/\mu} \quad (2.)$$

Expressions for the source term Λ_p in layer p may be found in literature [Stamnes *et al.*, 1988]. In the first term, the up-welling radiance I_{surf} at BOA follows directly from the surface boundary condition.

5.2.3.3 Computation of Jacobians

The retrieval requires the Jacobian of the TOA radiance with respect to all elements of the state vector. These state elements influence the radiance through their effect on the optical input parameters (the vertical grid of optical thickness, single-scatter albedo and phase function moments). We define the state vector element x_q (x_q might be the ozone partial column in that layer, or e.g. the aerosol optical thickness) affecting the optical input parameters in layer q only. We write down the explicit derivative of Eq. (1.):

$$\frac{\partial I(0, \mu, \phi)}{\partial x_q} = \frac{\partial}{\partial x_q} \left\{ I_{surf}(\tau_p, \mu, \phi) e^{-\tau_p/\mu} + \sum_{p=1}^P \Lambda_p(\mu, \phi) e^{-\tau_{p-1}/\mu} \right\} \quad (3.)$$

Using the chain rule for differentiation, this derivative can be written as a function of the derivatives of the surface radiance, the optical thickness values and the layer source functions. Further repeated applications of the chain-rule then express these components in terms of the derivatives $\frac{\partial \Delta \tau_p}{\partial x_p}$, $\frac{\partial \omega_p}{\partial x_p}$ and

$\frac{\partial \beta_{l,p}}{\partial x_p}$ which express the basic variation in atmospheric optical properties. These

derivatives are the basic input for the model, depending on the specific choice of x_q .

Because of the linearity of the discrete ordinate equations, it can be shown that the boundary value problem for the derivatives of the integration constants and the constants themselves is essentially the same; only the right-hand source vector is different. Integration constant derivatives are then simply found by back-substitution; there is no need for further matrix inversion. The Jacobian can be determined exactly without any additional numerical computation other than that used to determine the original radiance solution; the RTM needs to be called just once to deliver the complete set of radiance derivatives in addition to the radiance itself. This represents a very substantial saving in computational effort compared with the repeated calls to the RTM required to calculate Jacobians using finite-difference methods. Also, since the Jacobian solution is analytic, there are no problems about accuracy that often arise when dealing with ad-hoc finite-difference estimates. Further details on the linearisation procedure and the derivation of Jacobians can be found in [Spurr *et al.*, 2001] for the general N -stream case, and [van Oss & Spurr, 2002] for the faster 4 and 6-stream analytic solutions.

5.2.3.4 Sphericity correction at large viewing angle

For large off-nadir viewing directions, the ordinary pseudo-spherical calculation is insufficiently accurate for viewing zenith angles greater than about 30°-35°. To

remedy this, we must employ source function integration, but along the line-of-sight instead of the vertical. A straightforward sphericity correction procedure has been developed for this situation [*van Oss & Spurr, 2002*]. The technique is similar to that found in *Caudill et al. [1997]*. The exact single scatter radiance / Jacobian solutions are found explicitly for all solar rays scattering once into the line-of-sight. LIDORTA multiple scatter source function contributions and derivatives are calculated for the geometries at the start and finish of the atmospheric line of sight path; values for other points are interpolated with no significant loss of accuracy. GOME-1 has a maximum off-nadir viewing angle of about 30° for nominal viewing, for the polar viewing mode this angle reaches 50° . GOME-2 has a range of $\pm 45^\circ$ for nominal scan angle movements.

5.2.3.5 Polarisation Correction

Ideally, radiative transfer in the UV/visible should be modelled using the full Stokes 4-vector representation. It has been shown that the scalar RTM approximation (only the intensity component of the Stokes vector) introduces errors up to 10% for the radiance at TOA [*Mischenko et al., 1994, Stammes, 1994, Lacis et al., 1998*]. The error is largest when solar and viewing directions are at right angles. The effect of this error source on retrieved ozone profiles is large enough to require a correction for the polarisation RTM error [*Spurr 2001; Hasekamp et al. 2002*]. Vector RT models are presently too time-consuming to be useful in an operational algorithm such as the present one for GOME (~16 times slower for the full Stokes vector treatment). We use the scalar LIDORTA model, with a lookup table containing polarisation errors for all relevant conditions to be encountered. A doubling/adding vector model [*de Haan et al. 1987*] is used to construct the look-up table; entries are expressed as the relative difference in the radiances computed in the 4-vector and scalar-only treatments. The look-up table is classified by geometry (10 solar zenith angles, 7 viewing angles and 3 azimuth angles), surface albedo (8), surface pressure (3), ozone profile (20 global profiles from the TOMS version 8 climatology for 4 seasons and 5 latitude zones), total ozone (3) and wavelengths (116, between 290 and 400 nm). After correction, there is a residual radiance error due to the unknown profile shape. This error reaches a maximum of 0.3% around 320 nm. Figure 4 shows a subset of the look-up table.

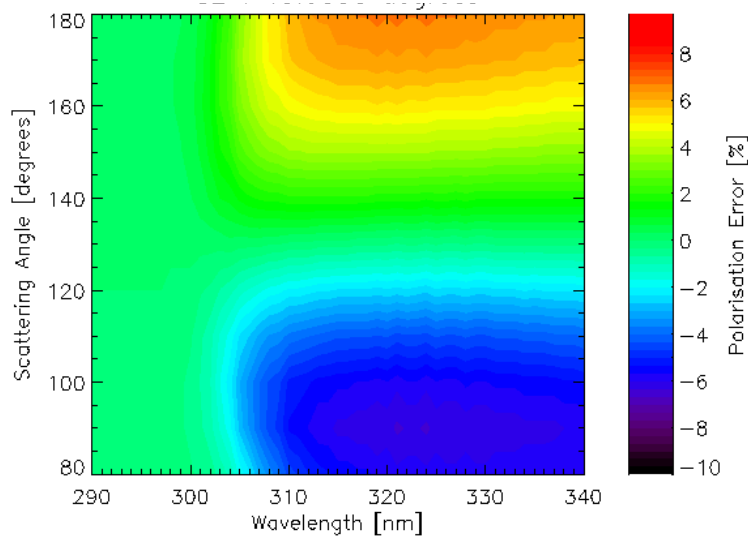


Figure 4: Error in the radiance due to neglecting polarisation in the radiative transfer calculations [%] as a function of wavelength and scattering angle, for solar zenith angle = 40 °, surface albedo = 0.3, surface pressure = 1000 hPa, latitude range = N30°-N50°, Season = JFM.

5.2.3.6 Raman scattering

Inelastic rotational Raman scattering (RRS) by air molecules is predominantly responsible for the observed filling-in of solar Fraunhofer lines and trace gas absorption features in UV and visible backscatter spectra. RRS-induced Fraunhofer and telluric filling-in is known collectively as the Ring effect. In ground-based and remote sensing UV/visible atmospheric reflectance spectra, the Ring effect shows up as small-amplitude distortions that follow Fraunhofer lines and absorption signatures. These interference structures are important sources of error and they can be treated in the spectral fitting of trace gas column and profile amounts.

Most UV-VIS retrieval algorithms only account for the filling in of the Fraunhofer lines. There is a clear need for an improved correction for the filling-in of ozone absorption structures for ozone retrievals. It has been shown that this effect, when not accounted for, can lead to errors in the ozone column of several percent [Spurr, 2003; de Haan, 2003]. Figure 5 shows the error on the reflectance when Raman scattering is not accounted for, for ten values of the ozone column. The ozone profiles are drawn from the TOMS V8 climatology for the month of July. The difference in Raman error between the ten cases can be attributed to the filling-in of ozone structures. This directly affects the ozone retrievals since it strongly correlates with the variation in the spectrum due to a variation in ozone.

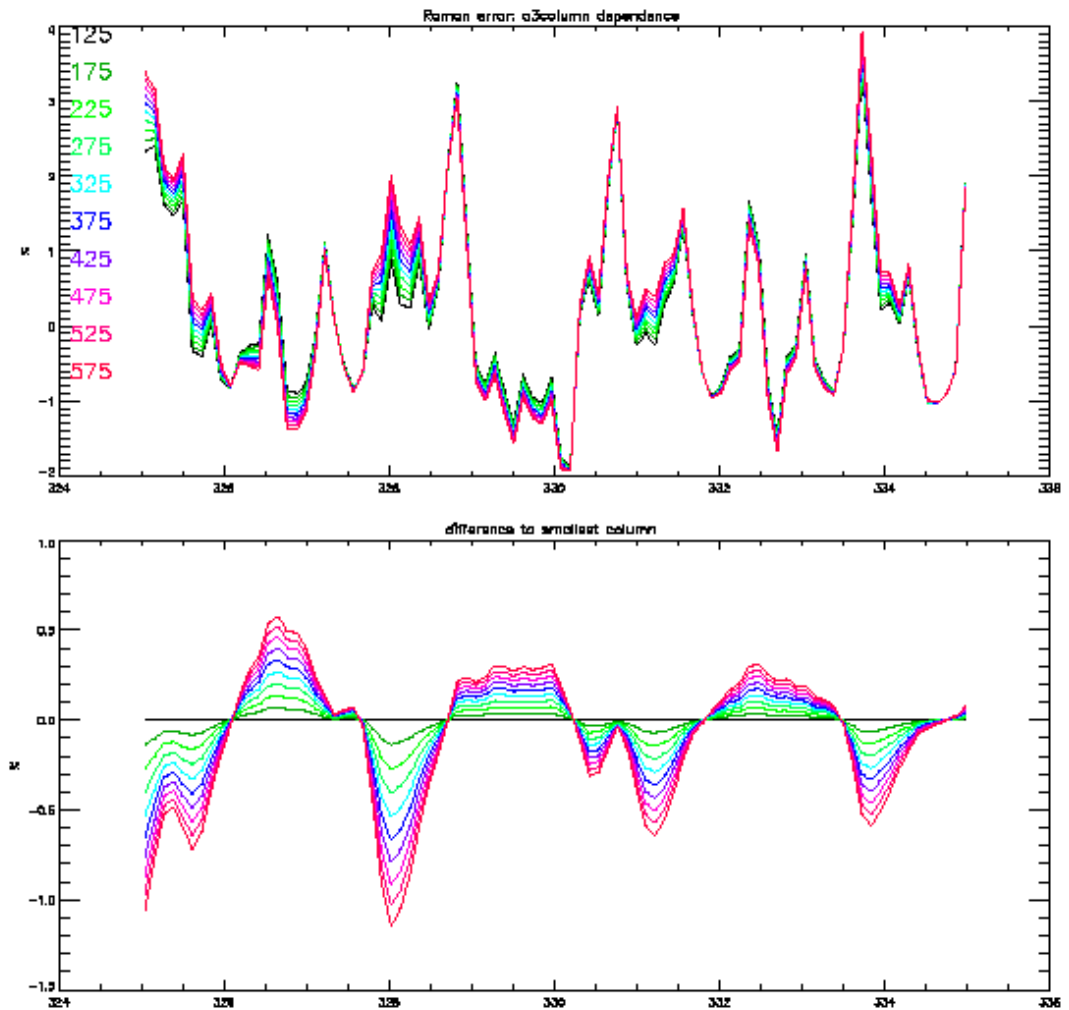


Figure 5: TOP: Error in reflectance when Raman scattering is not accounted for ("Filling") for ten TOMS V8 ozone profiles; total column is shown in DU. Bottom: Differences with respect to Raman error for 125 DU.

For total ozone retrieval using the DOAS method simple but effective treatments have recently been introduced by *de Haan* [2003] and by *van Roozendael* [2002]. The two methods differ somewhat, but they are based on the same principle. A similar treatment for ozone profile retrieval has recently been suggested by *de Haan* [2004].

The detected radiance is separated into a contribution from elastic scattering only (Cabannes) and a contribution from radiation that has been Raman-inelastically scattered once or more. It turns out that the fraction that has been inelastically scattered twice or more is negligible for the relevant wavelength range.

Let R_{Cab} be the reflectance when the molecules scatter according to the Cabannes scattering law, while the extinction by the molecules is that of Rayleigh scattering. This means that the single scattering albedo of the molecules is about 0.96 for Cabannes scattering. Let R_{Ray} be the reflectance for 'normal' Rayleigh

scattering, which has a single scattering albedo of one. We note that Rayleigh scattering has a slightly different phase function than Cabannes scattering.

The wavelength average amount of the inelastic reflectance is simply given by $R_{Ray} - R_{Cab}$. In absence of absorption features, i.e. spectrally smooth absorption on a wavelength scale of a few nm, the spectral fine structure of the scattered light is given by (for a plane parallel atmosphere)

$$I(\lambda) = R_{Cab}(\lambda)F_0(\lambda) + (R_{Ray}(\lambda) - R_{Cab}(\lambda))F_{Ring}(\lambda) \quad (4.)$$

where

$F_0(\lambda)$ is the incident solar flux (measured perpendicularly to the beam)

$F_{Ring}(\lambda)$ is the solar spectrum convoluted with the Raman lines, specifically

$$F_{Ring}(\lambda) = \frac{\sum_{k=1}^K \sigma_k(\lambda - \Delta\lambda_k) F_0(\lambda - \Delta\lambda_k)}{\sum_{k=1}^K \sigma_k(\lambda - \Delta\lambda_k)} \quad (5.)$$

where $\sigma_k(\lambda - \Delta\lambda_k)$ are the scattering cross sections for rotational Raman scattering and $\Delta\lambda_k$ are the corresponding wavelength shifts.

However, for ozone there are absorption features and we do have to account for them. If we assume that all absorption features are scrambled in the same way as in Eq. (5) we have

$$R_R(\lambda)F_{Ring}(\lambda) \Big|_{\text{abs and sun scrambled}} = \frac{\sum_{k=1}^K \sigma_k(\lambda - \Delta\lambda_k) R_R(\lambda - \Delta\lambda_k) F_0(\lambda - \Delta\lambda_k)}{\sum_{k=1}^K \sigma_k(\lambda - \Delta\lambda_k)} \quad (6.)$$

where $R_R(\lambda) = R_{Ray}(\lambda) - R_{Cab}(\lambda)$.

In the atmosphere, absorption features get scrambled that are build-up before rotational Raman scattering takes place, not features that are build up after Raman scattering. Therefore, the proper approximation is to use a weighted average of Eqs. (5) and (6), with the geometrical airmass factors as weights :

$$I(\lambda) = R_{Cab}(\lambda)F_0(\lambda) + \frac{\sum_{k=1}^K [\mu^{-1}R_R(\lambda) + \mu_0^{-1}R_R(\lambda - \Delta\lambda_k)]\sigma_k(\lambda - \Delta\lambda_k)F_0(\lambda - \Delta\lambda_k)}{(\mu_0^{-1} + \mu^{-1})\sum_{k=1}^K \sigma_k(\lambda - \Delta\lambda_k)} \quad (7.)$$

μ and μ_0 are the cosines of the viewing and solar zenith angle respectively.

The consequence of this approach is that the RTM now has to run twice for every wavelength: to compute $R_{Cab}(\lambda)$ and $R_R(\lambda)$. A more exact treatment of Raman scattering would, however, cost much more.

5.2.3.7 Computing the instrument radiance measurement

The RTM provides the reflectance R for a set of wavelengths $\{\lambda_i\}$. Multiplied by the reference solar irradiance at the same wavelength this gives I , the earthshine radiance. The radiance measurement of the instrument is computed by convolution with the slit function:

$$S_i = \int_0^{\infty} R_i(\lambda')I(\lambda')d\lambda' \quad (8.)$$

Here, S_i is the radiance value for spectral pixel i as it will appear in the level-1 product and R_i is the instrument response function (slit function) for pixel i . The evaluation of the integral in Eq. (8) requires radiance values at many wavelengths within the slit function envelope, since the radiance spectrum varies considerably due to the highly structured solar irradiance spectrum. However the reflectance spectrum varies considerably less and interpolation can be used to compute the reflectance for intermediate wavelengths.

Since the computational effort of the retrieval algorithm scales linearly with the number of wavelengths for which the RTM has to be run, a logical approach is to:

1. select a minimal set of wavelength $\{\lambda^{\text{OPTM}}_i\}$ for which the reflectance is computed with the RTM,
2. use (spline) interpolation to obtain the reflectance at the fine wavelength grid needed for the slit function convolution $\{\lambda^{\text{slit}}_i\}$
3. multiply with a reference solar irradiance spectrum, given at the $\{\lambda^{\text{slit}}_i\}$ grid to obtain the radiance spectrum
4. Evaluate the convolution, Eq. (8)

The task is to find the optimal set $\{\lambda^{\text{OPTM}}_i\}$. Figure 6 shows the error in radiance computation for different samplings of the reflectance calculation $\{\lambda^{\text{OPTM}}_i\}$. The Figure shows that a sampling of about 1 nm is enough for the region < 300 nm, but for larger wavelengths the instrument sampling becomes important. Even the

smallest sampling in the image (0.11 nm, yellow line) gives errors larger than 0.5% for some wavelengths. This reflects the spectral variation of the ozone cross-section, see Figure 1.

The reference solar irradiance spectrum used in Opera is derived from the “Kitt Peak” (*Chance and Spurr, 1997*) by *Voors et al. (2006)*. This spectrum is down-scaled by a user-configurable factor before use for calculation of simulated solar spectra or calculation of simulated radiances on a high spectral resolution.

The slit function for GOME-1 has a Gaussian shape with a fixed FWHM per channel. For GOME-2 the slit function can be treated in multiple ways: 1) the slit function shapes conform the recommendations in TNO/TPD GOME-2 FM203, Issue 3 Slit_Function (document MO-TR-TPD-GO-0097i3.pdf, pages 100 -- 104; APPENDIX C Details slit-function of the FPAs), with a fixed channel averaged FWHM; or 2) the tabulated Slit Function Stimulus response per instrument as given by RAL (Ref: Siddans et al. Analysis of GOME-2 Slit function Measurements: Final Report Eumetsat Contract No. EUM/CO/04/1298/RM (for GOME-2 on Metop-A)). Software versions later than v1.28 use the latter method.

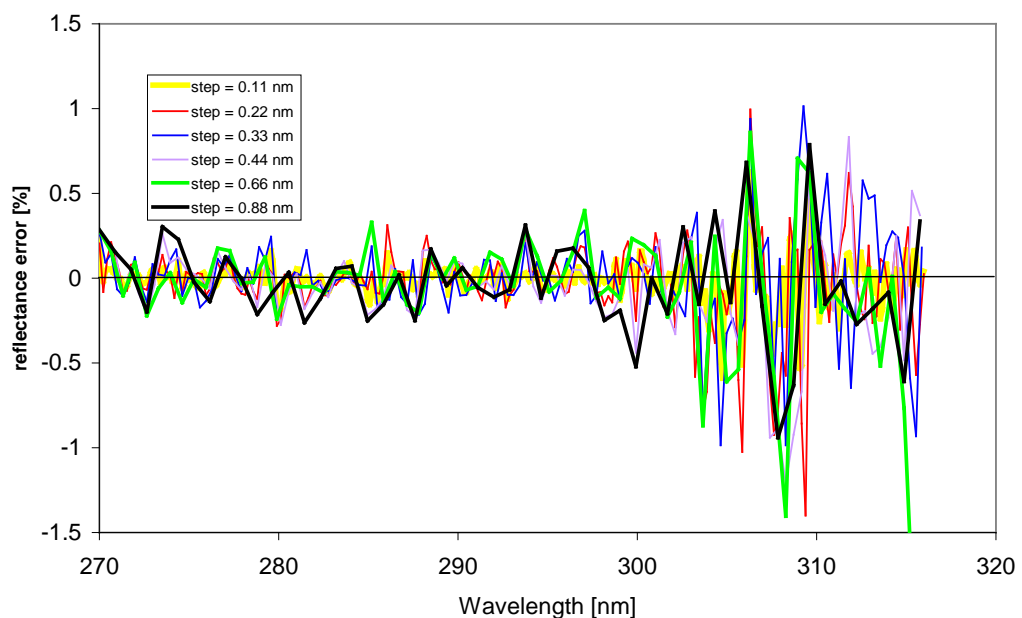


Figure 6: error in radiance computation for different samplings of the reflectance calculation.

5.3 Inversion using Optimal Estimation

When the number of profile elements to be retrieved exceeds the number of independent profile elements that can be retrieved, a naive least squares fitting produces meaningless results for real and noisy spectra. Small-scale variations in atmospheric quantities that are poorly constrained by the measurement will cause noise amplification, resulting in spurious retrieved values often showing

strong oscillations. Two methods for circumventing this ill conditioning can be distinguished: (i) limiting the number of profile elements to be retrieved, and (ii) regularising the inversion problem. The first option can be realised by fitting profile elements at a limited number of carefully chosen levels in accordance with the restricted profile information in the measurement. This would require a specification of the shape of the profile between the layers. The use of a fixed vertical grid would be non-optimal for most cases.

Regularisation suppresses noise amplification by using information from a source other than the measurement. Regularisation is achieved by adding a second term to the least squares cost function J to be minimised:

$$J = (\mathbf{y}_m - F(\mathbf{x}))^T S_y^{-1} (\mathbf{y}_m - F(\mathbf{x})) + R(\mathbf{x}) \quad (9.)$$

Here, \mathbf{y}_m is the measurement vector of radiances, \mathbf{x} is the state vector of parameters to be retrieved, $F(\mathbf{x})$ is the radiance calculated by the forward model and S_y is the error covariance matrix. $R(\mathbf{x})$ is some function of the state that returns a large amplitude for 'undesirable' solutions. Two choices for the regularisation are commonly used for atmospheric retrievals; these are the Phillips-Tikhonov [Hasekamp & Landgraf, 2001] and Optimal Estimation (OE) methods [Rodgers, 2000]. In OE, the $R(\mathbf{x})$ term is derived from the application of Bayes' theorem. This states that the probability density function (*PDF*) of the state is proportional to the *PDF* of the measurement given the state, multiplied by the *PDF* of the state prior to the measurement. The measurement changes the likely outcomes for the state vector elements, since it provides extra information on top of that already available from prior information. When the *PDFs* are all Gaussian distributions, the most probable state (the Optimal Estimate) minimises the cost function Eq. (9.) with the regularisation term: $R(\mathbf{x}) = (\mathbf{x} - \mathbf{x}_a)^T S_a^{-1} (\mathbf{x} - \mathbf{x}_a)$. Here \mathbf{x}_a is the *a priori* state vector and S_a the prior covariance matrix.

The optimal estimate minimises the cost function with the regularisation term: Eq. (9). This value can be found by iteratively applying:

$$\begin{aligned} \mathbf{x}_{i+1} &= \mathbf{x}_a + D_y [\mathbf{y}_m - \mathbf{y}_i - K_i (\mathbf{x}_a - \mathbf{x}_i)] \quad \text{with} \quad D_y = S_{i+1} K_i^T S_y^{-1} \quad \text{and} \\ S_{i+1} &= (K_i^T S_y^{-1} K_i + S_a^{-1})^{-1} \end{aligned} \quad (10.)$$

where $K_i = (\partial F / \partial \mathbf{x})_i$ is the Jacobian at state \mathbf{x}_i ; K^T the transpose of the Jacobian, $\mathbf{y}_i = F(\mathbf{x}_i)$ and \mathbf{x}_{i+1} is the updated state vector. The matrix D_y is known as the matrix of contribution functions; the solution error covariance is given by S_{i+1} . The iteration starts with some initial estimate of the state, and terminates when convergence has been reached. We employ two convergence criteria, according to Rodgers [2000]. The primary criterion is that the difference between the error-weighted lengths of two consecutive state vectors, i.e. $S_x^{-1/2} (\mathbf{x}_i - \mathbf{x}_{i-1})$, should be below a fixed threshold. Investigations have shown that a maximum difference of 1% in gives good results for all cases. The second convergence criterion to be met is that the change in the cost function between two consecutive iterations should be less than some predefined value. We have adopted 1%, which appears to work fine. These two criteria combine convergence tests in both state space and measurement space. The final value of the solution error covariance matrix is the main source of diagnostic information for the retrieval.

The actual computation of the optimal estimate is performed by using linear transformations $\mathbf{x}' = V^T S_a^{-1/2}(\mathbf{x} - \mathbf{x}_i)$ and $\mathbf{y}' = U^T S_y^{-1/2}(\mathbf{y}_m - \mathbf{y}_i)$, where U and V are unitary matrices resulting from the singular value decomposition (SVD) of the scaled Jacobian: $K' = S_y^{-1/2} K S_a^{1/2}$. In terms of primed variables, elements of the optimal estimate vector are given by:

$$x'_{\text{OE},j} = \frac{\lambda_j y'_j + x'_{j,a}}{\lambda_j^2 + 1} \quad (11.)$$

Here, λ_j are the singular values resulting from the SVD. A useful measure of the number of independent linear combinations of the state vector elements that can be retrieved from the addition of measurements is given by the degrees-of-freedom-for-signal (*DFS*) indicator, defined by:

$$DFS = \sum_j \frac{\lambda_j^2}{1 + \lambda_j^2} \quad (12.)$$

If N is the dimension of the state vector, we have $DFS = N$ if the measurement completely determines the state, and $DFS = 0$ if there is no information at all in the measurement.

6. IMPLEMENTATION OF THE OPERATIONAL OZONE PROFILE RETRIEVAL ALGORITHM

In the previous chapter the main components of the algorithm are described. This chapter treats all choices that have to be made that affect both accuracy of the retrieved profile and speed of the algorithm. Since the algorithm applies an RTM for a large number of wavelengths, it is time consuming and any measure that can reduce the computational time and at the same time does not lead to a too high consequence for the accuracy should be pursued.

6.1 Retrieval and model grid

The ozone profile is retrieved on an almost fixed pressure grid consisting of a number of layers (e.g.: 20, 32 or 40), logarithmically spaced between 1000 and 0.1 hPa. Almost, because, the actual surface pressure replaces one or more levels below it and the level closest to the cloud top is replaced by the latter. The vertical grid on which all geophysical profiles are defined is equal to this grid.

6.2 Level 1 Input and usage

6.2.1 Level 1b

The basic level 1B data comprise a calibrated solar spectrum and spectra of calibrated geolocated radiances; each spectrum comes with a wavelength grid, error estimates and status flags. In the geolocation record, solar and line-of-sight viewing angles are specified at a reference height h_0 (h_0 =surface for GOME-2), satellite height and earth radius are specified for the sub-satellite point, and for each nadir-view footprint the corner and centre co-ordinates (surface latitude and longitude) are given. The vertical pressure grid is adjusted to the surface pressure and to the cloud top pressure. If the cloud top pressure is higher than the surface pressure then the clouds are put at the surface (with the surface pressure kept as leading value). The adjustment is flagged in the QualityInput flags record.

Since the algorithm uses information from the wavelength region between 265 and 330 nm, it is necessary to combine information from Band 1a and Bands 1b and 2a/b. These bands have different integration times. All Band 1b and band 2a/b pixels within the Band 1a pixel can be averaged to obtain the spectrum from which the ozone profile for the Band 1a ground pixel can be derived. Alternatively, individual Band-1b sized pixels can be combined with the enclosing Band-1a pixel in order for higher spatial resolution retrievals. The spectra from the Band-1a size pixel will generally give information on the stratospheric part of the atmosphere and the spectra from the Band 1b-2b size pixel will produce additional for the tropospheric part.

6.2.2 South Atlantic Anomaly

The South Atlantic Anomaly (SAA) causes spikes in the spectrum, especially in Band 1a. These spectral pixels will not be taken into account in the Optimal Estimation inversion step of the ozone profile algorithm. The reduced number of useful wavelengths in the spectrum will decrease the amount of information as e.g. expressed in the DFS.

The way the 'SAA filter' works for Software Versions up to v1.26 is as follows: We start at a certain wavelength (say 290 nm) where it is assumed that the spectrum is not perturbed by the highly energetic particles in the SAA. This wavelength is called the reference wavelength. From that reference wavelength we compare the radiance of the next shorter wavelength. If the radiance is more than 3-sigma higher than the radiance of the reference wavelength then we flag it as invalid. If the radiance is less than 85% of the reference wavelength then it is also flagged as invalid. If the radiance is within the +3-sigma -- 85% range, then we update the reference wavelength/radiance to the current wavelength and continue to shorter wavelengths. If a configurable number of flags have been set, we stop and flag the rest of the shorter wavelengths as well. The procedure is depicted in Figure 7. The start reference wavelength, the top error margin, the bottom margin and the number of flagged radiances before the removal of the rest of the shorter wavelength spectrum occurs can be user-configured. The parameters used in the SAA filter are given in the table below.

For ozone profiles retrieved with Software Version 1.28 (and later) the method is similar as described above, but the radiance used as a reference is no longer the individual radiance but a box car average radiance across a configurable number of spectral pixels is used. This has the advantage that peaks and underflows do affect the reference to a lesser degree which results in a more stable filter. The new parameters (v1.28+) have been empirically determined.

Table 2; SAA filter settings for particular software versions

SAA Filter Parameter	v1.26 and before	v1.28 and after
Start wavelength	290 nm	290 nm
Sigma factor	3.0	4.0 (for PFS>5.3)
Max reduction factor	0.15 (85%)	2.0
Max spike count	50	30
Box car size	--	21

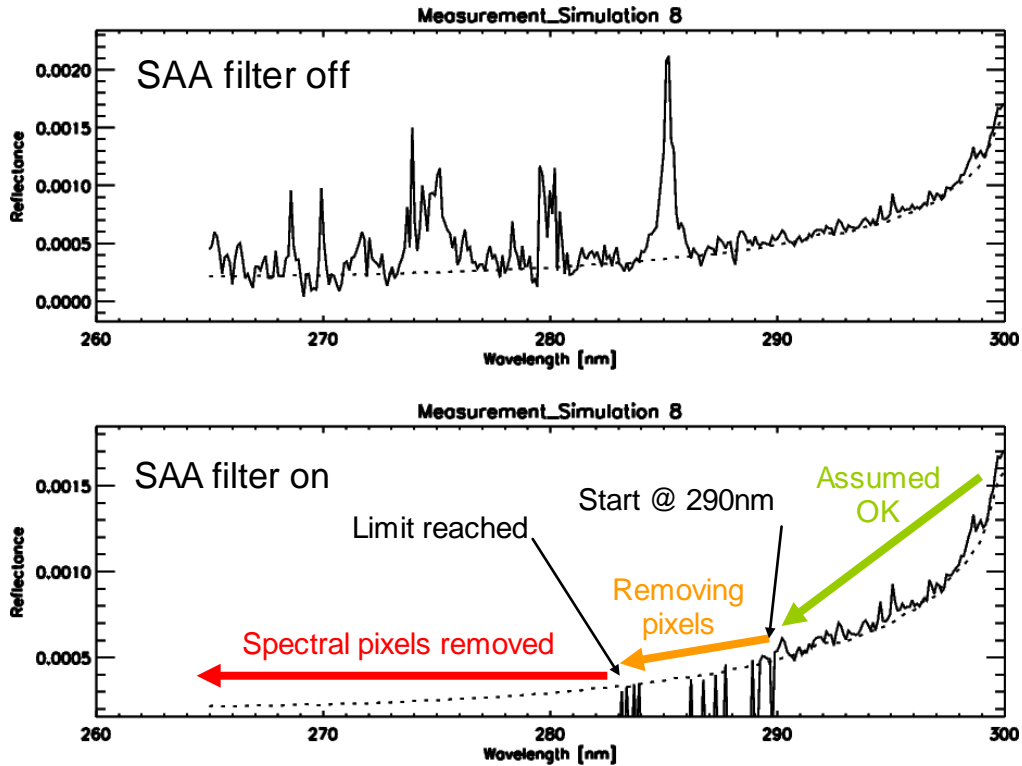


Figure 7: Effect of the SAA filter on the inclusion/use of spectral measurements in the Optimal Estimation inversion step within the Ozone Profile Retrieval Algorithm.

6.2.3 Additive Offset

Optionally, an additional offset can be applied to the fitting windows (and this value can be fitted as part of the normal state vector). The additional offset CEA0 is an additive value applied to the radiance. The value fitted can be $X * 1.0E+9$ photons or a factor $X * \text{the radiance value at the lowest wavelength in the first window}$. The offset can be coupled between fitting windows (e.g.: fitted in Window-1 and applied to window 2 as well). Tests have shown that this offset is required in at least Channel-1 to compensate/correct between the measured and simulated spectrum.

6.3 Level 2 output of the vertical ozone profile retrieval

Opera generates one or more output files per orbit: a full HDF5 product for offline distribution and a file containing limited information in BUFR format for Near Real Time (NRT).

- Full product, format HDF5

The product contains the retrieved profile, the full error covariance matrix, the retrieval noise covariance matrix, the *a priori* profile the averaging kernels and the retrieved auxiliary parameters, like surface or cloud albedo. Also included are: geolocation, spectral windows used and retrieval diagnostics, like number of iterations, spectral fit indicators.

The ozone profile is reported as partial columns, in Dobson Units, between the user provided pressure levels between and including surface pressure and 0.1 hPa. For cloudy and partially cloudy scenes, the cloud-top pressure replaces the nearest pressure level.

- Minimum information, format BUFR

This is like the SBUV BUFR product: containing the ozone partial columns and error estimates. Averaging kernels and error covariance matrices are not included and have to be extracted from the full HDF5 product if needed due to lack of appropriate descriptors in the standard ECMWF BUFR software, at this time.

A full description of the Opera output products will be given in the Product User Manual for the Near Real Time and Offline Ozone Profile.

6.4 Definition of the state vector and *a priori*

The set of parameters to be retrieved from the level 1 measurements, the state vector, includes ozone partial column for each model layer and the surface or cloud albedo for the spectral window at the largest wavelength side. The albedo of the other windows are coupled to this albedo.

For the *a priori* ozone profile, there are a few options, described in section 5.2.2.1. For the cross-correlations we use a fixed matrix for all months and latitudes based on a re-examination of the source data of the climatology [Timmermans, 2000].

6.5 Performance Considerations

6.5.1 Forward Model Efficiency

The computational effort of the RTM and the accuracy of the computed radiance depends strongly on the number of streams and the number of layers. It is therefore important to minimize the number of streams and layers while still meeting the accuracy requirements.

Number of streams

LIDORTA is fast and efficient with $N = 4$ or 6 discrete ordinate streams (CPU varies roughly with N^2); the use of analytic discrete ordinate solutions also improves the efficiency. For the vast majority of atmospheric scenarios relevant to GOME ozone profile retrieval, four streams are usually sufficient to ensure that

radiances and weighting functions are calculated to a level of accuracy that matches the measurement uncertainty. In scenarios where there is a strong aerosol presence in the troposphere, and for retrievals that use wavelengths beyond 320 nm, the six-stream option may be necessary to achieve accuracy levels of 0.5% for radiances. The nominal setting of the number of streams in the Opera software is four.

Number of layers

For short wavelengths in the UV where single scattering dominates (<295 nm), a minimum of 10 layers per pressure decade is required for single scatter radiance errors <0.1%. This is the reason for often using a 40-layer grid.

However, for the multiple-scatter LIDORTA computation, a smaller number of layers is sufficient to give the required accuracy level for the wavelength ranges and atmospheric and viewing conditions relevant to this algorithm. Since the speed of a LIDORTA run is proportional to the cube of the number of layers, the use of a coarse grid for multiple scatter represents a large gain in computational speed.

Figure 8 and Figure 9 show the error in the radiance due to a limited number of layers. The radiance obtained for 40 layers can be regarded as the truth. The pressure levels bounding the layers are logarithmically distributed between 1000 and 0.1 hPa. A separate computation of the single and the multiple scattered radiance allows a reduction of only the multiple scattering computation, which has the largest impact on algorithm speed. The figures illustrate that we may reduce the number of layers to 20 for the multiple scattering computation while still retaining an accuracy < 0.2% for all cases.

In the case of a highly reflecting surface (such as snow or ice), the radiation field becomes more uniform. The effect on the accuracy is smaller than the effect for varying solar zenith angle as shown below.

We conclude that a number of 40 layers would be necessary to achieve an accuracy < 0.2% for all wavelengths. Reducing the layers to 20 for the multiple scattering computation only is allowed since it does not lead to worse accuracy.

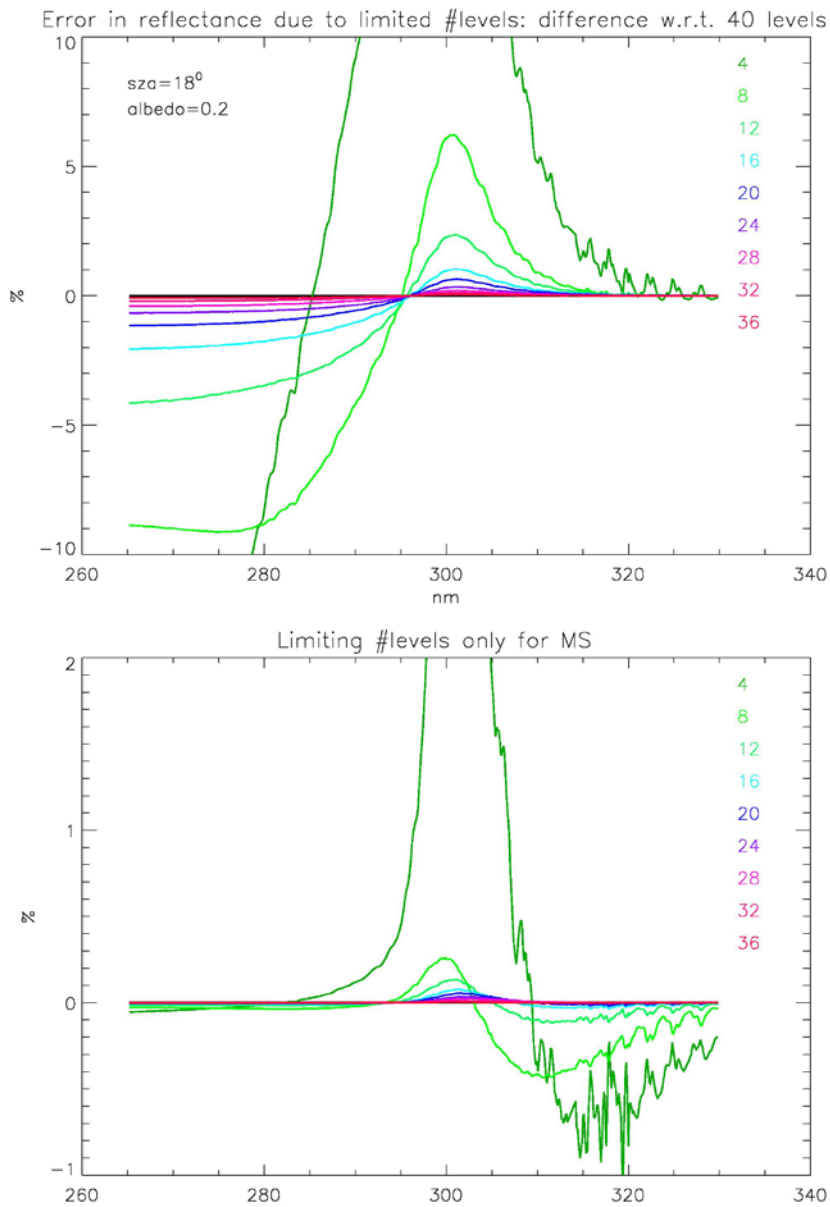


Figure 8: Error in TOA radiance due to limited number of layers. Top panel: layering for complete radiative transfer computation; Bottom: layering for multiple scattering part. A solar zenith angle of 18° is used.

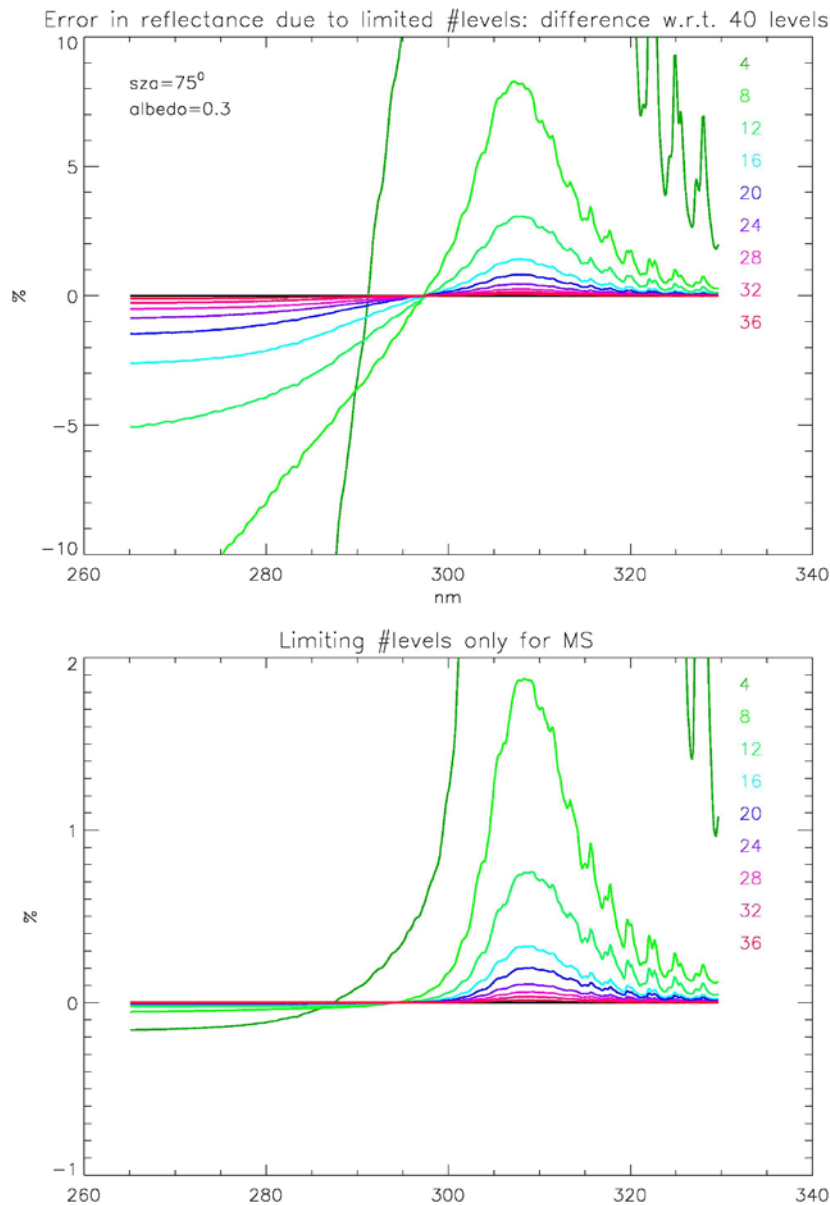


Figure 9: Same as previous figure, but for a solar zenith angle of 75°.

6.5.2 Fitting Window

The DFS indicator Eq. (12.) can be used to optimise the upper wavelength limit of the fitting window [van Oss & Spurr, 2001a]. Figure 10 shows DFS values plotted against upper wavelength limit for two solar zenith angles with two different temperature profiles: a tropical and an Antarctic profile. Also, the decrease of the DFS, in case a 0.5% measurement error is added to the noise (taking into account calibration, model and interpolation errors) is shown. The lower wavelength limit is fixed at 270 nm. There is a substantial increase in information with the inclusion of wavelengths above 300 nm, and the tropospheric

temperature sensitivity becomes apparent above ~313 nm. There is little increase in DFS beyond about 330 nm, suggesting that the inclusion of wavelengths above this threshold will not significantly enhance the retrieval.

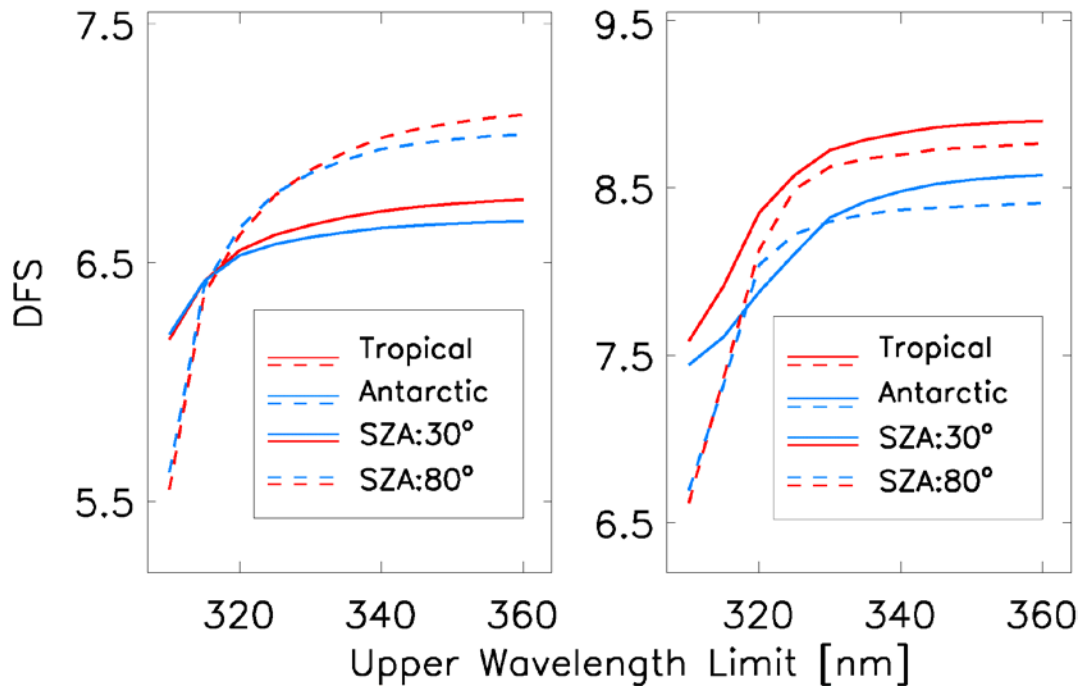


Figure 10: Degrees of Freedom for signal (DFS) as a function of upper wavelength limit, for two values of the solar zenith angle and two ozone profiles. The right panel treats the case where the measurement error consist of the instrumental noise only, whilst for the left panel the error has been increased by 0.5% of the radiance to account for calibration, forward model error and interpolation error. We may conclude that beyond 330 nm no significant increase in DFS is seen and that the increase in measurement error limits the temperature sensitivity of the retrieval.

If the upper wavelength limit increases, the influence of other error sources on the retrieval increases. There is a trade-off between the extra information that is present in the spectra by considering longer wavelengths and the enhanced error due to these sources. The results of the error analysis allow us to make a sensible choice of upper wavelength of 330 nm.

7. VERTICAL OZONE PROFILE INFORMATION

7.1 Averaging kernels

The averaging kernel (A) relates the retrieved profile (\hat{x}) to the true (x_{true}) and the *a priori* profile (x_a) according to:

$$\hat{x} - x_a = A(x_{true} - x_a) \quad (13.)$$

The averaging kernel quantifies the degree at which profile information on the given vertical grid has been extracted from the spectral measurement. It suppresses vertical structures in the true anomaly ($x_{true} - x_a$) on which no information is present in the measurement.

An example of a set of averaging kernels is shown in Figure 11. Here, the kernels are scaled with the *a priori* profile:

$$A_{ij}(scaled) = \frac{(\hat{x}_i - x_{a,i}) / x_{a,i}}{(x_{true,j} - x_{a,j}) / x_{a,j}} \quad (14.)$$

This way, the kernels for different layers can be more easily compared.

For the high solar zenith angle scene the profile information in the troposphere is reduced, but in the higher stratosphere there is more information. The kernels have their smallest width around 40 kilometres. For the low solar zenith angle situation they are a bit smaller and higher peaked.

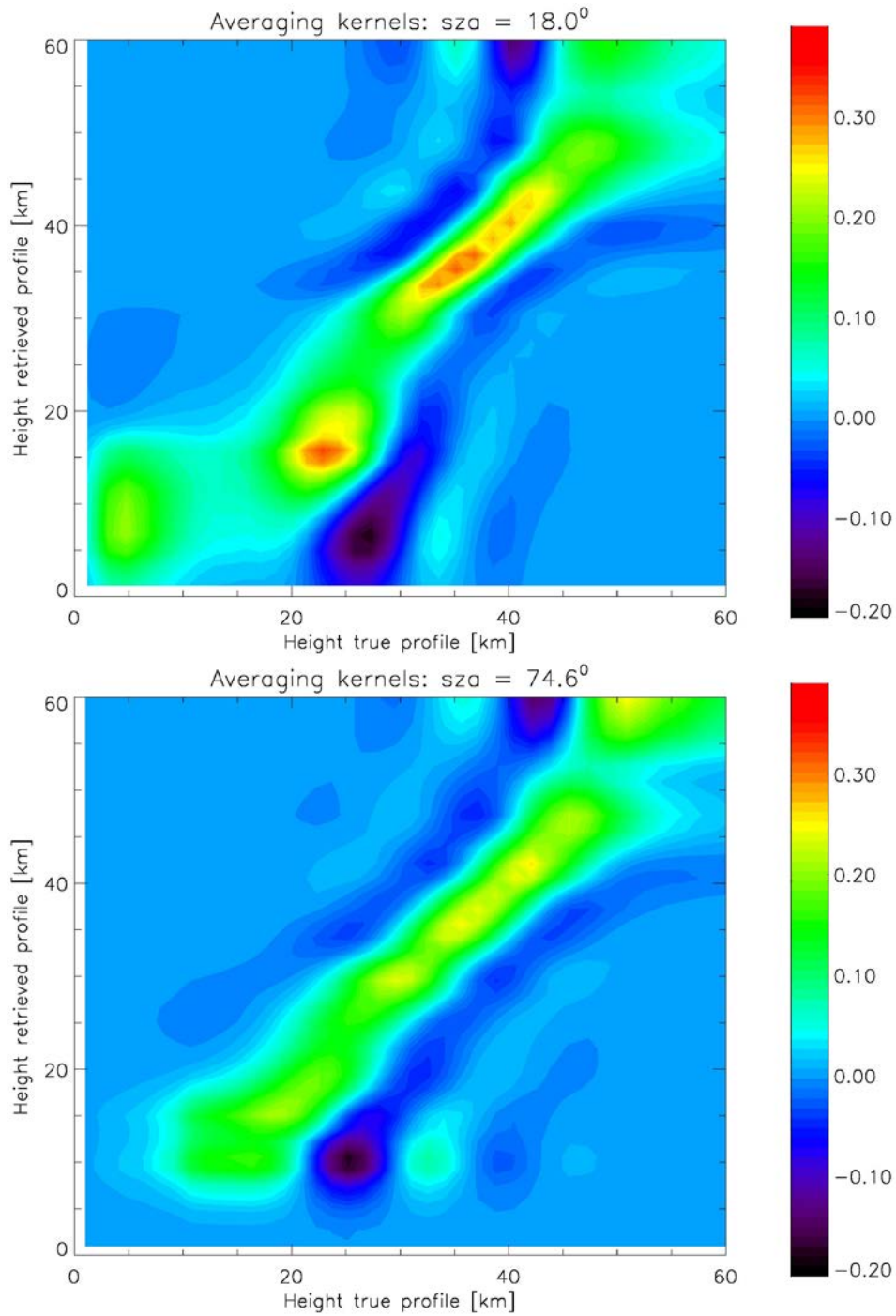


Figure 11: Averaging kernels for two values of the solar zenith angle (sza). The kernels are scaled with the *a priori* profile.

Note the dependence of the averaging kernels on the *a priori* and measurements errors:

$$A = \left(K^T S_y^{-1} K + S_a^{-1} \right)^{-1} K^T S_y^{-1} K \quad (15.)$$

For decreasing measurement errors, the averaging kernel converges to the unit matrix, for increasing errors the matrix elements tend to zero. For the *a priori* errors it is the other way around. This implies that the behavior of the averaging kernel, and thereby the vertical resolution of the profile (in terms of separable pieces/layers of information) depends on the magnitude of the *a priori* errors: smaller *a priori* errors mean the weight given to the *a priori* profile and vertical correlations as expressed in the *a priori* error covariance matrix, is increased. In the case that the *a priori* information has poor vertical resolution this will be reflected in the averaging kernels. In other words, smaller *a priori* errors lead to less retrieved independent pieces of information from the measurement. The sampling stays the same (i.e.: the number of vertical model layers). This is illustrated in Figure 12 where the *a priori* profile errors are scaled with a height-constant factor, starting from the standard value from the climatology. The factor ranges from 0.1 to 9.9. The width of the kernels becomes smaller for increasing *a priori* errors, reflecting the fact that the retrieval extracts more information from the measurement and less from the *a priori*. Note that the price that has to be paid for the better resolution is the larger retrieval error. Also, the inversion may not be regularized enough. The consequence of this is that measurement errors begin to affect the profile shape (noise amplification) and the retrieval does not converge anymore.

We adhere to the spirit of the statistical basis (Bayes' theorem) of optimal estimation and chose for the *a priori* error covariance realistic data obtained from independent measurements on ozone profiles. Tuning the *a priori* error such that a favourable balance between resolution and retrieval error, or *a priori* and measurement information, is obtained would violate the statistical basis and be similar to the L-curve criterion used in Phillips-Tikhonov regularization [Hasekamp & Landgraf 2001]

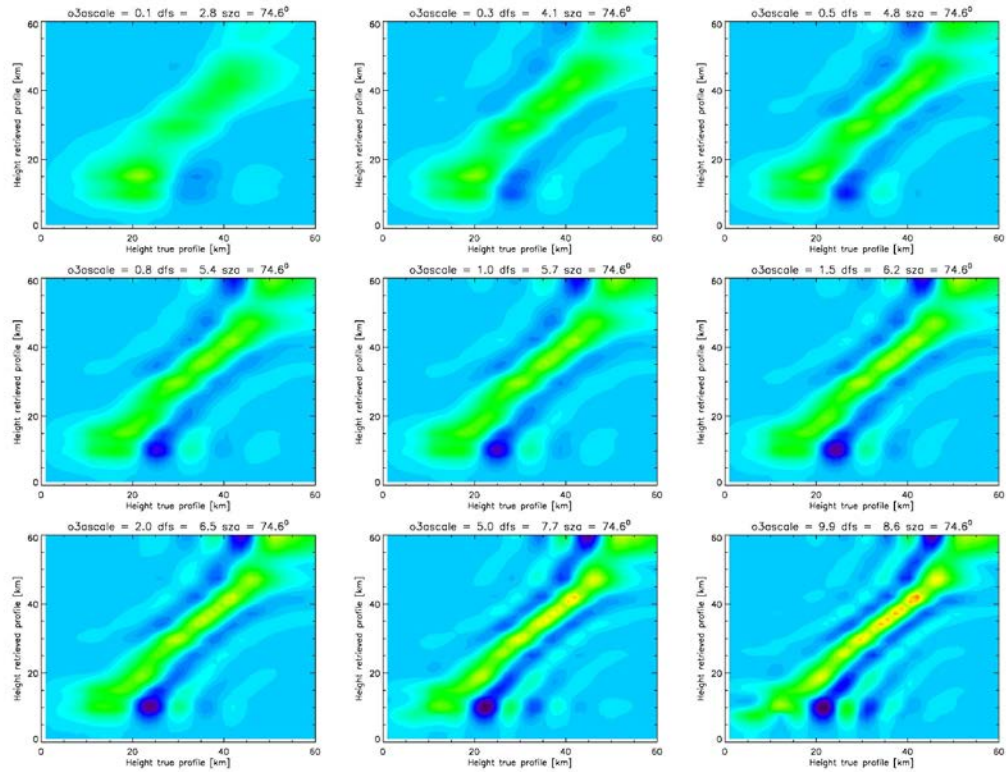


Figure 12: Averaging kernels for nine values of the a priori error. The errors for all layers are scaled with a constant factor. This factor ranges from 0.1 (top left) to 9.9 (bottom right). Clearly the increase in vertical resolution is seen for the larger a priori errors.

8. EVALUATION OF THE ACCURACY OF THE OZONE PROFILE USING ERROR ANALYSIS

The accuracy of the retrieved profile is established by identification and quantification of the main error sources and their effect on the profile.

Following *Rodgers* [2000] we express the optimal estimate of the state x_{OE} in terms of the “true” value of the state vector x_{true} plus errors:

$$\begin{aligned} x_{OE} &= x_{true} + (A - I)(x_{true} - x_a) + D_y \varepsilon_y \\ D_y &= S_x K^T S_y^{-1} \end{aligned} \quad (16.)$$

The matrix D_y is known as the matrix of contribution functions. I is the identity operator in state space. The second term on the RHS of Eq. (16.) denotes the *smoothing error*. The remaining error $D_y \varepsilon_y$ can be split into three components: $D_y \varepsilon_y = D_y \varepsilon_{me} + D_y \varepsilon_{fme} + D_y \varepsilon_{mpe}$, with the following definition of errors in ‘measurement space’:

ε_{me} : measurement error: random and systematic,

ε_{fme} : forward model error,

ε_{mpe} : model parameter error.

We discuss these four error components below.

Smoothing Error

The smoothing error gives the deviation between the true and retrieved state caused by the use of *a priori* information. It vanishes in the limiting case when the *a priori* error increases to infinity and the retrieved profile is extracted from the measurement only. The presence of smoothing error indicates that the retrieved profile is not an estimate of the true profile itself, but rather an estimate of a well-defined transformation of the true profile. When validating the retrieved profile, it is sometimes convenient to omit the smoothing error contribution. If so, this requires knowledge of the averaging kernels and the *a priori* to be able to relate the retrieval results to the truth. The contribution S_{se} to the solution covariance from this error component can be estimated by using the *a priori* covariance matrix for the state covariance: $S_{se} = (A - I) S_a (A - I)^T$. Alternatively, the smoothing error can be calculated from $S_{se} = S_{total} - S_{noise}$.

Measurement error contribution

This error is the total of all errors in the spectral measurement, random and systematic. The random (noise) contribution to ε_y generates a solution covariance component of the retrieval noise, $S_{noise} = D_y S_y D_y^T$, contributing to the retrieved profile error. The systematic error in the spectrum (Δf) generates a profile error $\varepsilon_{me} = D_y \Delta f$.

Forward model errors

This error may be due to an incorrect or inaccurate representation of the physics of the problem. This is a systematic source of error. The systematic error in the model (Δf) generates a profile error $\varepsilon_{me} = D_y \Delta f$.

Model parameter errors

The retrieval error due to this source of uncertainty is given by $\varepsilon_{mpe} = K_b \Delta b$, where K_b is the sensitivity of the forward model to the model parameter b and Δb is the error in the model parameter itself. If Δb is a random error, the solution error covariance component for this model parameter error is given by $S_{parameter} = D_y K_b S_b K_b^T D_y^T$. Model parameter errors can be both random and systematic.

8.1 Test data set: Input configuration

The error computation is performed for for a number of cases that cover the full range of possible measurements. We have:

- two latitudes 15N and 45N
- two cloud fractions 0.0 and 1.0,
- two solar zenith angles θ_o (30°, 75°), defined at h0,
- two relative azimuth angles ϕ (0°, 180°) and
- two viewing angles θ (10°, 50°), defined at h0
- two seasons: summer and winter (i.e.: to two different *a priori* ozone profiles)

The following parameters are the same for all scenarios:

- surface albedo (0.05),
- cloud top albedo (0.8),
- cloud top pressure (700 hPa) and
- wavelength range (265 – 330 nm).

This constitutes a total of 64 scenarios. *A priori* ozone profiles are selected from the ozone climatology from *McPeters et al (2007)*.

8.2 Error analysis results

The calculations are done on 40 layers, but we aggregate these to 12 layer intervals in the tables. The errors are RMS values for all scenarios combined.

Systematic errors are computed by mapping the error in the spectrum to a profile error using the contribution function (gain matrix).

Table 1 gives the RMS of the *a priori* and the smoothing errors using the ozone climatology from *McPeters et al (2007)* [ML] and *Fortuin and Kelder (1999)* [FK].

Table 2 shows the resulting errors on the ozone profile as a result of several anticipated errors in the GOME-2 Level 1b Earthshine spectrum. These measurement errors are:

- A wavelength calibration error of 1/30th pixel, both for the short [270 – 300 nm] and the long wavelength region [300-330 nm]. (**systematic**)

- An offset error in the radiance with a magnitude of 2% of the radiance at 270 nm. (**systematic**)
- A multiplicative error of 1% in the radiance at all wavelengths. (**systematic**)

Table 3 shows the errors in the profile due to *systematic* errors in parameters of the Forward Model. We consider:

- An error in the Rayleigh cross section of 1% at all wavelengths
- An error in the ozone cross section of 1% at all wavelengths
- An error in the temperature of 5K at all layers
- An error in the cloud-top of 100 hPa

Table 4 gives the profile errors due to errors in the radiative transfer model:

- the 4- stream approximation in the LIDORTA model compared to the 6 stream model,
- neglect of Rotational Raman scattering (Ring effect), excluding effect of RRS on atmospheric absorption.
- neglect of polarisation

Figure 13 shows the *a priori*, total, noise and smoothing errors for two different solar zenith angles (30.0 and 75.0 degrees), and two surface albedo values (0.05 and 0.80). The other input parameters are fixed: a clear sky, summer season at 45N, LOS 10.0, relative azimuth 0.0 and, when not varied, the SZA 30.0 and surface albedo 0.05.

Table 1: List of a priori and smoothing errors for indicated layers. Errors are given in percent. The columns refer to layer intervals bounded by the pressure levels indicated in the first row.

	1000-700	700-500	500-300	300-200	200-100	100-70	70-30	30-10	10-5	5-1	1-0.3	0.3-0.0
A priori error ML O3 clim	23.2	22.9	30.2	46.7	34.4	23.7	10.7	7.3	7.9	9.1	10.6	16.1
A priori error FK O3 clim	28.4	24.4	35.3	49.9	44.8	28.9	13.9	10.9	13.9	13.9	13.8	14.9
Smoothing error ML O3 clim	19.2	17.4	21.5	30.2	21.1	12.6	5.2	3.3	3.0	2.4	5.2	12.1
Smoothing error FK O3 clim	24.5	19.2	24.8	31.3	25.5	14.2	6.3	4.1	3.9	4.0	5.8	9.77

Table 2: List of measurement errors for indicated layers. Errors are given in percent. All errors are regarded as systematic. The columns refer to layers bounded by the pressure levels indicated in the first row.

	1000-700	700-500	500-300	300-200	200-100	100-70	70-30	30-10	10-5	5-1	1-0.3	0.3-0.0
λ -scale [270-300 nm] 1/30 pix	0.2	0.2	0.2	0.2	0.2	0.2	0.1	0.1	0.1	<0.1	<0.1	<0.1
λ -scale [300-330 nm] 1/30 pix	0.4	0.5	0.5	0.5	0.5	0.4	0.1	0.1	0.1	<0.1	<0.1	<0.1
Radiance offset 2% at 270 nm	<0.1	<0.1	0.1	0.2	0.2	0.2	<0.1	<0.1	<0.1	1.2	2.3	2.9
Radiance multiplicative 1%	6.1	6.5	6.4	6.3	2.3	1.7	1.2	0.6	1.0	1.5	1.3	1.2

Table 3: Profile errors due to systematic model parameter errors. Errors are given in percent. The columns refer to layers bounded by the pressure levels indicated in the first row.

	1000-700	700-500	500-300	300-200	200-100	100-70	70-30	30-10	10-5	5-1	1-0.3	0.3-0.0
Rayleigh Cross sect. 1%	2.8	2.8	2.6	2.5	1.3	1.3	0.6	0.5	1.0	1.5	1.3	1.2
Ozone Cross sect. 1%	0.8	1.0	1.6	2.6	2.5	2.5	1.3	0.8	0.9	1.0	0.9	0.8
Temperature 5K	9.4	10.4	11.2	10.4	7.1	8.7	3.3	1.5	1.4	0.6	0.2	0.2
Cloud-top 100 hPa	3.8	4.2	5.0	6.4	3.4	1.5	0.5	0.2	0.2	0.2	<0.1	<0.1

Table 4: Profile errors due to forward model errors. Errors are given in percent. All errors are regarded as systematic. The columns refer to layers bounded by the pressure levels indicated in the first row.

	1000-700	700-500	500-300	300-200	200-100	100-70	70-30	30-10	10-5	5-1	1-0.3	0.3-0.0
4-stream error	4.0	4.3	4.6	5.4	2.6	1.6	0.9	0.3	0.3	0.1	0.0	0.0
Neglect of Ring	3.4	3.7	3.4	4.6	5.5	6.0	2.0	0.8	0.4	0.3	0.3	0.2
Neglect of polarization	28.3	29.5	29.9	32.5	14.8	4.6	3.4	1.7	1.1	0.5	0.3	0.3

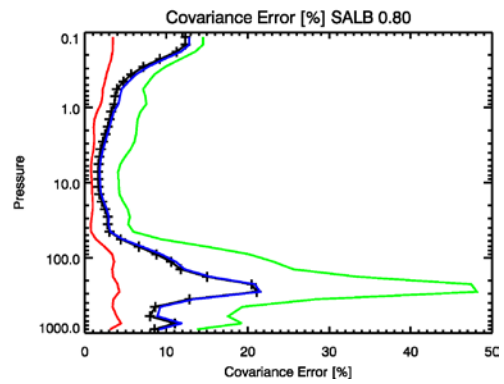
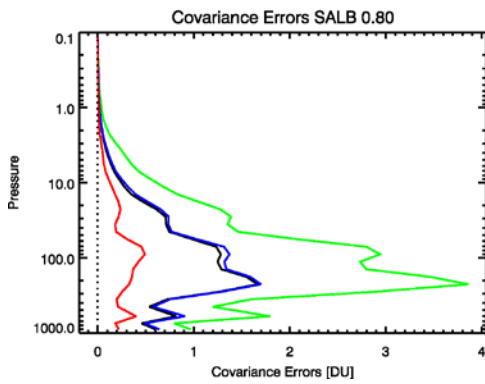
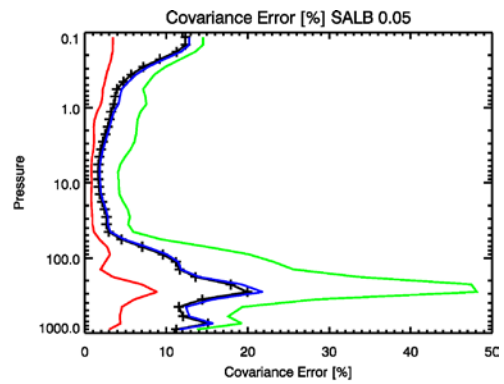
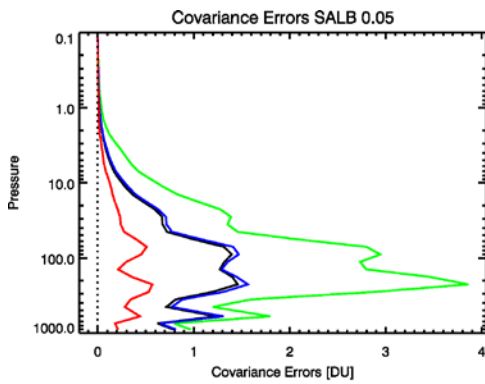
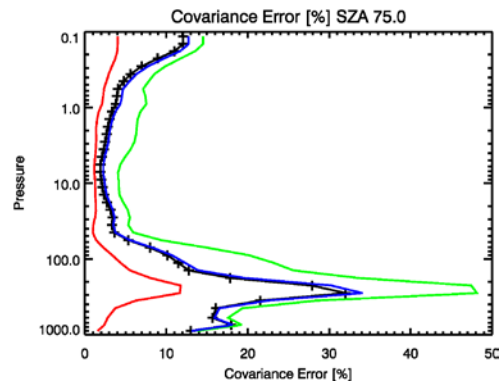
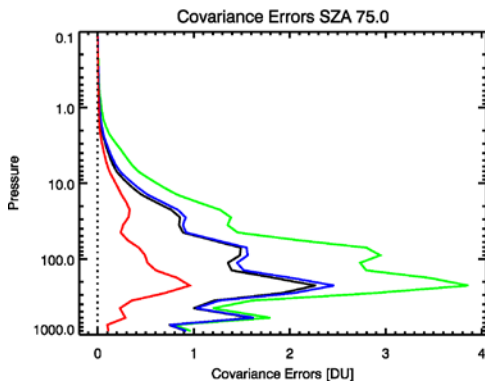
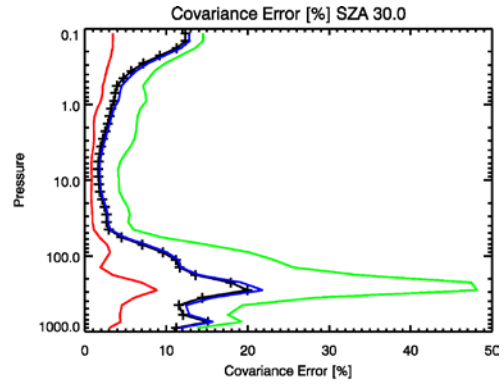
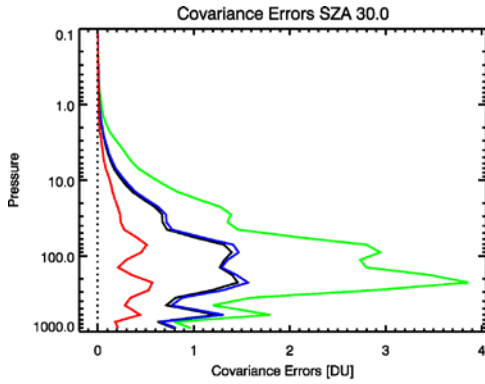


Figure 13: Covariance errors in DU and percent, for two SZA angles and two surface albedo values. Green: a priori error, blue: total error, black: smoothing error, red: noise error

The results indicate the following dominant error sources exceed the 5% level:

- Spectral calibration,
- Rayleigh cross section,
- Temperature
- Cloud top pressure
- 4-stream error,
- Neglect of Ring,
- Neglect of polarization.

Some of these error sources can be reduced by:

- Incorporating accurate data of optical properties in the atmospheric forward model.
 - Using information on the temperature of the atmosphere from NWP models
 - Using 6-streams instead of 4.
 - The treatment of Raman scattering as outlined in Section 5.2.3.6.
 - Using a lookup table containing polarisation errors, Section 5.2.3.5
-

9. VERTICAL OZONE PROFILE VALIDATION

Validation of ozone profiles requires a statistical analysis of differences to co-located ozone profile measurements done by other means. These can be sondes, lidar, microwave, or other satellites (SAGE, SBUV, MLS, HALOE, POAM, GOME-1, SCIAMACHY or OMI). These measurements all have their vertical range that does not always cover the range of the reported GOME-2 profiles (surface to 0.1 hPa). The combination of sondes (0-30 km), lidars (10-50 km) and microwave (20–65 km) measured from the same location at the same day is very useful for the evaluation of the retrieved profiles. One has to take into account the spatial and temporal representativity of the ground based measurement with respect to the satellite retrieval (collocation differences, time integration differences, day/night measurements, etc).

An inter-comparison can be done in two ways: either using the averaging kernel on the collocated profile and thereby get rid of the smoothing error, or leave the collocated profile and take both the noise and smoothing error into account. This is best illustrated by Eq. (17.). If we do not use the averaging kernel the difference between the co-located (true) profile and the retrieved profile is given by:

$$x_{OE} - x_{true} = (A - I)(x_{true} - x_a) + D_y \varepsilon_y \quad (17.)$$

The first term on right-hand side of this equation is the smoothing error the second the retrieval noise, directly related to the measurements noise. In case we apply the averaging kernel to the collocated profile, and consider the profile anomalies (difference to *a priori*) instead of the profiles themselves, we can use:

$$(x_{OE} - x_a) - A(x_{true} - x_a) = D_y \varepsilon_y \quad (18.)$$

showing that the difference is only the retrieval noise.

Instead of directly comparing the sonde profile with the retrieved profile, either with, or without applying averaging kernels to the sonde, we differentiate between the limited capacity of the instrument to measure the ozone profile and the error in the product.

We consider the different terms in the relation between the retrieved, the *a priori* and the true (sonde) profile, cf. Eq. (18):

- True anomaly: $x_{true} - x_a$
- Detectable anomaly: $A(x_{true} - x_a)$
- Retrieved anomaly: $x_{retrieved} - x_a$

Note that the *a priori* is the climatological value, hence the term ‘anomaly’. The difference between (1) with (2) measures the capacity of the instrument to detect the anomaly, comparing (2) with (3) traces collocation errors and/or errors in the product, since they should be equal within the retrieval noise. By considering the anomaly instead of the profile itself, the possible confusion due to the dependence of the GOME profile on the *a priori* is avoided.

Figure 14 shows the GOME-1-sonde comparisons for one year of co-located Sodankylä measurements. The sonde profiles are limited to the altitude range below approximately 30 km. For the region above 30 km we assume the profile to be equal to the *a priori*, so the anomaly vanishes.

The comparisons between the first and second panels clearly show the fact that the GOME product is a smoothed version of the truth, reducing the amplitude of the a-normal structures and evaporating the small-scale anomalies.

The comparisons between the second and third panels show that there are still differences indicating the presence of co-location errors and/or errors in the level 1 product.

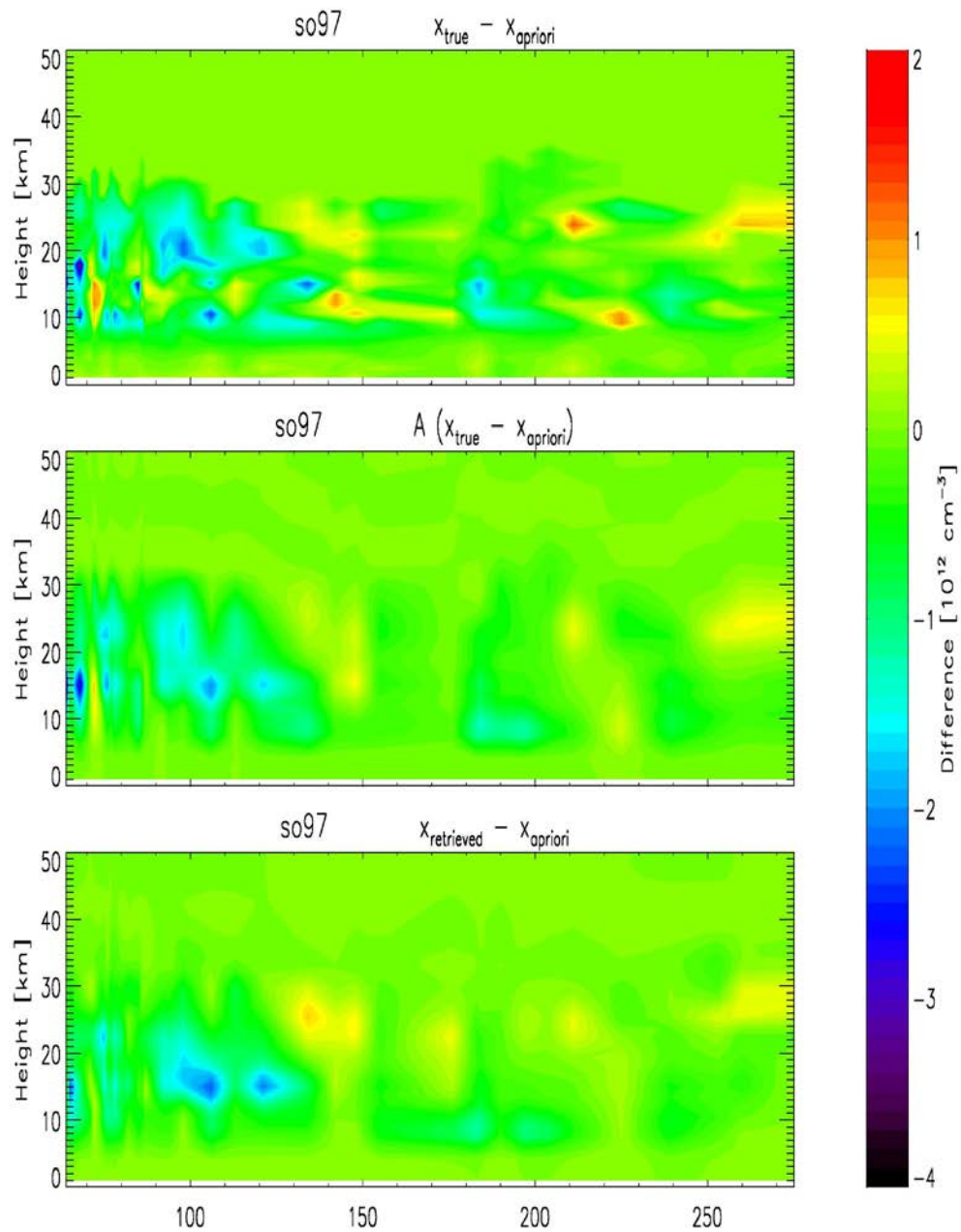


Figure 14: sonde ozone profile versus retrieved ozone profiles from GOME-1 for Sodankylä 1997. The horizontal axis is day of the year.

10. PARTIAL INTEGRATION OF VERTICAL OZONE PROFILES

10.1 General

The vertical ozone profile can be vertically integrated over a section of the atmosphere to calculate a partial column. Examples of these are the Tropospheric and the Stratospheric ozone column, but other sub-columns are also commonly used, such as the Surface to 500hPa column.

10.1.1 Calculation of partial ozone columns and its associated error

This section describes the methodology for vertically integrating profiles and calculating partial ozone columns and their associated error.

To get a partial column, the layers of the vertical profile are integrated (added up) following equation:

$$\text{Integrated profile} = \sum_{i=\text{BottomLayer}}^{\text{TopLayer}} O_3(i)w(i) \quad (19.)$$

In the equation *BottomLayer* and *TopLayer* are the indices to the model layers that include the bottom pressure and top pressure of the region to integrate. w is the layer-weight.

Given that the boundary of the RTM model layers usually do not coincide with the integration boundaries (e.g.: the tropopause height), a partial O₃ column needs to be added at the edges of the integration region. This is done using w , which is a vector containing the weights of the layers: $w_i = 1$ if fully included, $w_i = 0$ if not, and in case of partial layer inclusion the weight is between 0 and 1, based on the distance between the upper and lower 10-log pressure bounds of the layer. For example, if the tropopause level would be exactly above layer 5, the tropospheric column weighting vector w will look like (1,1,1,1,1,0, ..., 0,0) and the stratospheric column weighting vector like (0,0,0,0,0,1, ..., 1,1).

The error of the partial column is calculated by adding up the values of the covariance matrix as follows:

$$E = \bar{w}^T S \bar{w} \quad (20.)$$

Where E is the error (a scalar), S is the covariance matrix of the retrieved profile, and w is the same weights vector used above for the partial column.

10.1.2 Tropopause definitions

The atmosphere is separated vertically into two regimes by a strong temperature inversion that inhibits mixing of air between the troposphere and stratosphere. This inversion is called the tropopause. The height of the tropopause varies, depending on the latitude, season and regional effects of large scale meteorological systems. Usually the tropopause height is near 13 km in the tropics, comes down to about 10 km in mid-latitudes and can go as low as 7 km in polar areas with sustained subsidence.

The tropopause height definition used by the World Meteorological Organization is: “the lowest level at which the lapse rate decreases to 2 °C/km or less, provided that the average lapse rate between this level and all higher levels within 2 km does not exceed 2 °C/km” [WMO Manual on Codes, Vol.I.1-A, WMO–No. 306]. This definition is used here for the thermal tropopause.

Searching from the surface, we select the highest level for which the following formula holds:

$$\frac{dT}{dH} \leq -2.0^{\circ} C / km \quad (21.)$$

where dT is the temperature difference between layers and dH is the height difference.

Using Potential Vorticity, the tropopause can also be defined as the height/pressure closest to the surface where:

$$PV \geq 2.0 * 10^{-6} \quad (22.)$$

Where the PV is the absolute value of the potential vorticity (to avoid issues with positive at NH, and negative at SH). The actual threshold value can be configured in Opera.

Additionally, we require that the tropopause level is situated at a pressure smaller than 500 hPa to avoid lower level (ground or atmospheric) inversions and also that the tropopause is not at the first level in the model to avoid surface effects near high mountain ranges.

The thermal tropopause is a good measure in the tropics, but outside of the tropics the atmosphere is often isotherm for ~100hPa to high up in the stratosphere. Here the thermal tropopause fails and the PV based tropopause is better.

For latitudes < 19N/S the thermal tropopause is used (where valid). Between 19 and 36 degrees latitude (both in N and S direction), there is a linear transition between the thermal tropopause pressure and the PV based tropopause. From 36 degrees latitude to the pole the PV based tropopause pressure is used.

As an example, the tropopause pressure of the thermal tropopause and based on the PV are given in Figure 15.

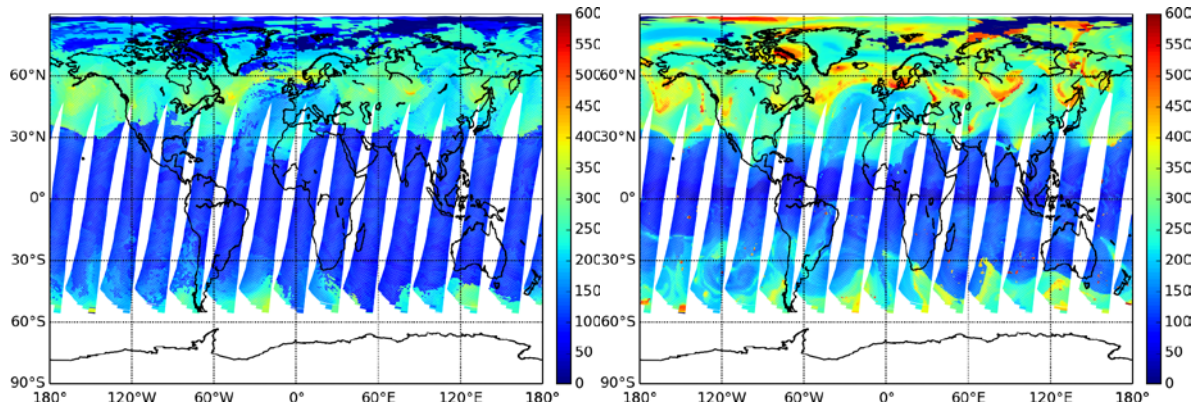


Figure 15: Tropopause pressure in hPa using the thermal definition (left) and PV definition (right) both based on ECMWF data if 2015-07-01.

10.1.3 Examples: the tropospheric and stratospheric columns.

The ‘full’ Tropospheric Ozone Column (TrOC) and Stratospheric Ozone Column (StrOC) can be derived from the retrieved vertical ozone profile by splitting the atmosphere at the tropopause and adding the partial ozone columns.

An example of the GOME-2 Integrated Vertical Ozone Profile (Total Ozone Column) and the Tropospheric, Stratospheric and Surf-500hPa Ozone Column on 2010-10-09 is shown in the next figures (Figure 16 and Figure 17):

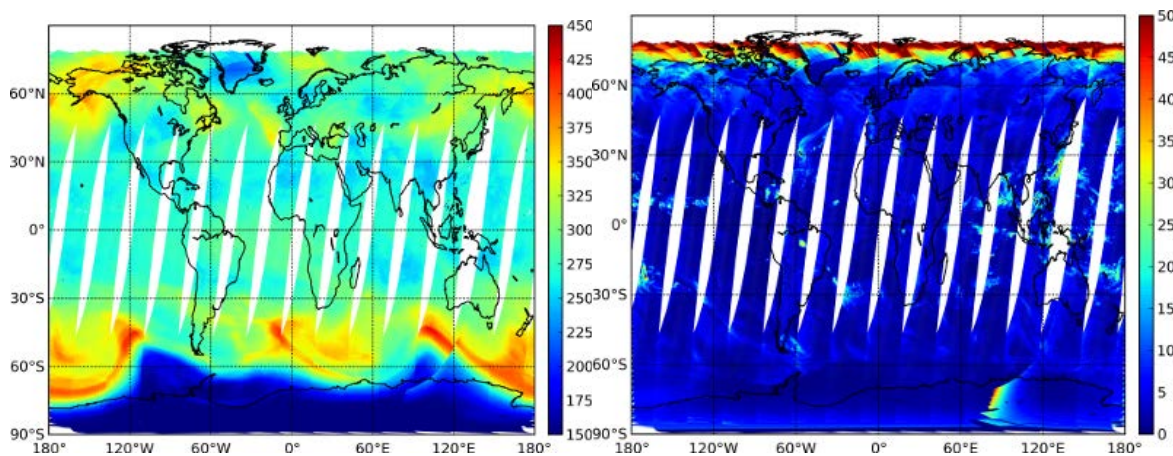


Figure 16: The Integrated Vertical Ozone Profile in DU (left) and the associated error in DU (right).

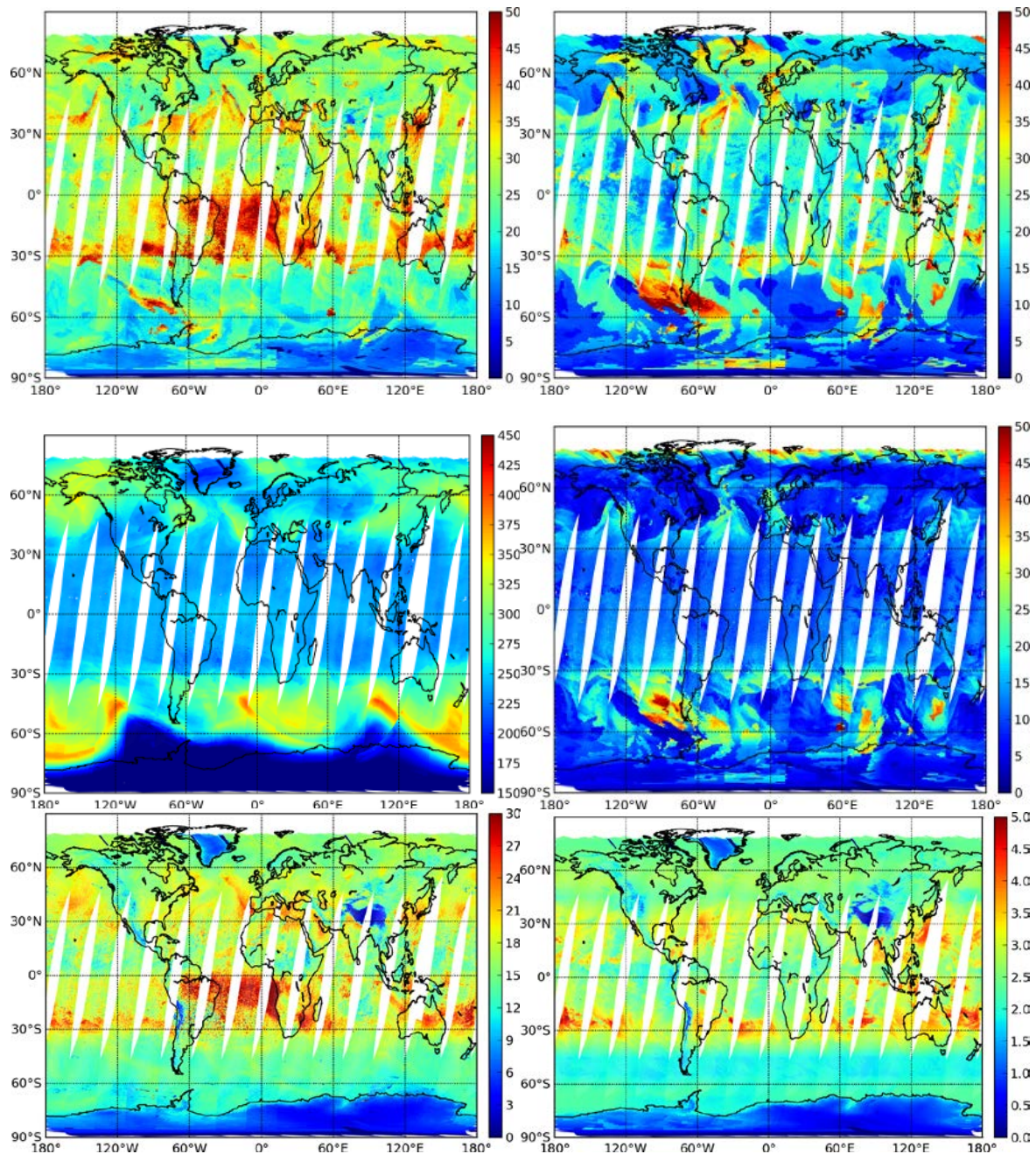


Figure 17: Top: the Tropospheric Ozone Column (left) and the associated error (right); Middle: the Stratospheric Ozone Column (left) and the associated error (right). Bottom: the Surf-500hPa Ozone Column (left) and the associated error (right).

10.2 Error sensitivity of the Tropospheric ozone column

The tropospheric ozone column is derived from the vertical ozone profile and therefore depends on its sensitivities as an intermediate product, described in earlier sections of this ATBD. One of the important things to keep in mind is that using the UV-VIS spectral range (265-330nm), the GOME-2 ozone profile retrieval

has good sensitivity in the stratosphere but is less sensitive to the lower part of the atmosphere compared to other instruments such as IASI. The expected calculated error on the GOME/GOME-2 TrOC is therefore often of the same order of magnitude as the TrOC value itself if calculated from the covariance matrix following equation 21. For the stratosphere there is a much better ratio of column versus the error value (a factor 8-10). The reason why the error of the total integrated column can be less than the sum of the TrOC and StrOC error is that the covariance matrix S in equation 21 also contains negative values, thus reducing the matrix/vector product.

The Tropospheric Ozone Column (TrOC) depends on the (errors in the) ozone profile. This includes uncertainty due to the unknown ozone amount below clouds for large cloud covers. In this situation the information below clouds comes from the *a priori* climatology used in the profile retrieval. Users are recommended to filter out cloud contaminated TrOC values based on the cloud fraction and cloud pressure values given in the output product. An example of the effect of cloud screening is shown in Figure 18 where one day and three days of data are shown with a cloud fraction below 20%. Even in the case of a three day average there are locations on Earth that have not been cloud free during the satellite overpass.

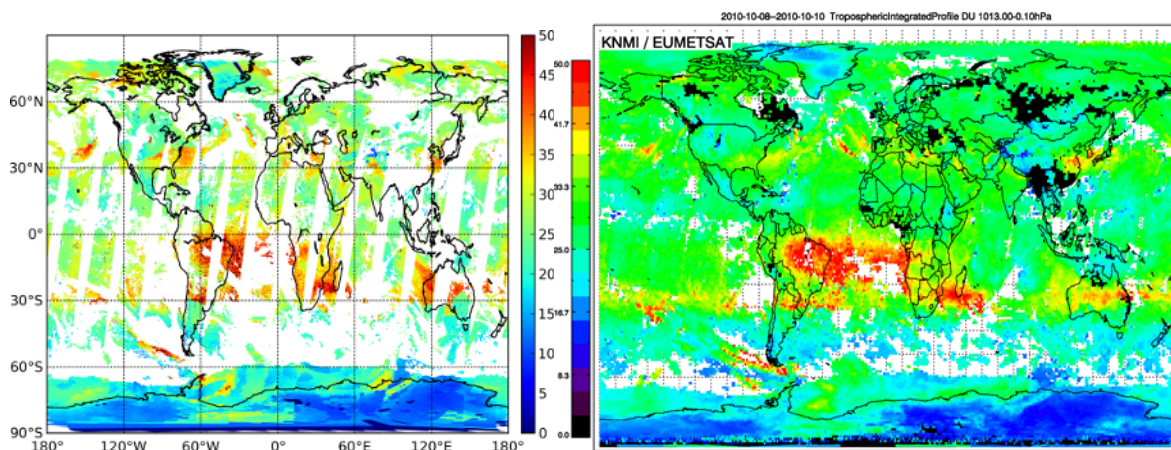


Figure 18: Left: Tropospheric ozone column screened for clouds ($C_f < 0.2$) for one day (2010-10-09); Right: Cloud screened TrOC averaged over three days (2010-10-08—2010-10-10)

Another source of error in the column product can be introduced via the selection of the tropopause pressure (Tp) from the temperature or PV values. The Tp is a free parameter in the calculation of partial columns, in this case the TrOC.

In Figure 19 below, we present two cases: one where the troposphere is assumed to coincide with a model level and where the tropopause level has been artificially lowered by one layer and one where it is increased by one layer. This gives an upper boundary of the expected difference in the full TrOC if the tropopause is not exactly between the layers. From the plots we can see that in absolute terms the difference is between -4 and +5 DU, which in relative terms ranges between minus 30% to plus 40% in some cases for the TrOC.

In Figure 20 to Figure 22 the initial time timeline comparisons with balloon reference data are shown in terms of absolute tropospheric ozone columns and relative differences for the station of Uccle (Belgium). In this case the balloon sondes are vertically integrated into a column (up to the tropopause and up to 500hPa respectively) and compared to the vertically integrated high resolution retrieved value. The bias in the relative difference is seasonally dependent and ranges between -30 and +20 percent with a standard deviation between +/- 40% with a few up to +/- 50% for the column up to the tropopause.

In Figure 23 a scatter plot shows an initial correlation between the TrOC from the profile retrieval versus the integrated ozone from balloon sondes for Wallops island.

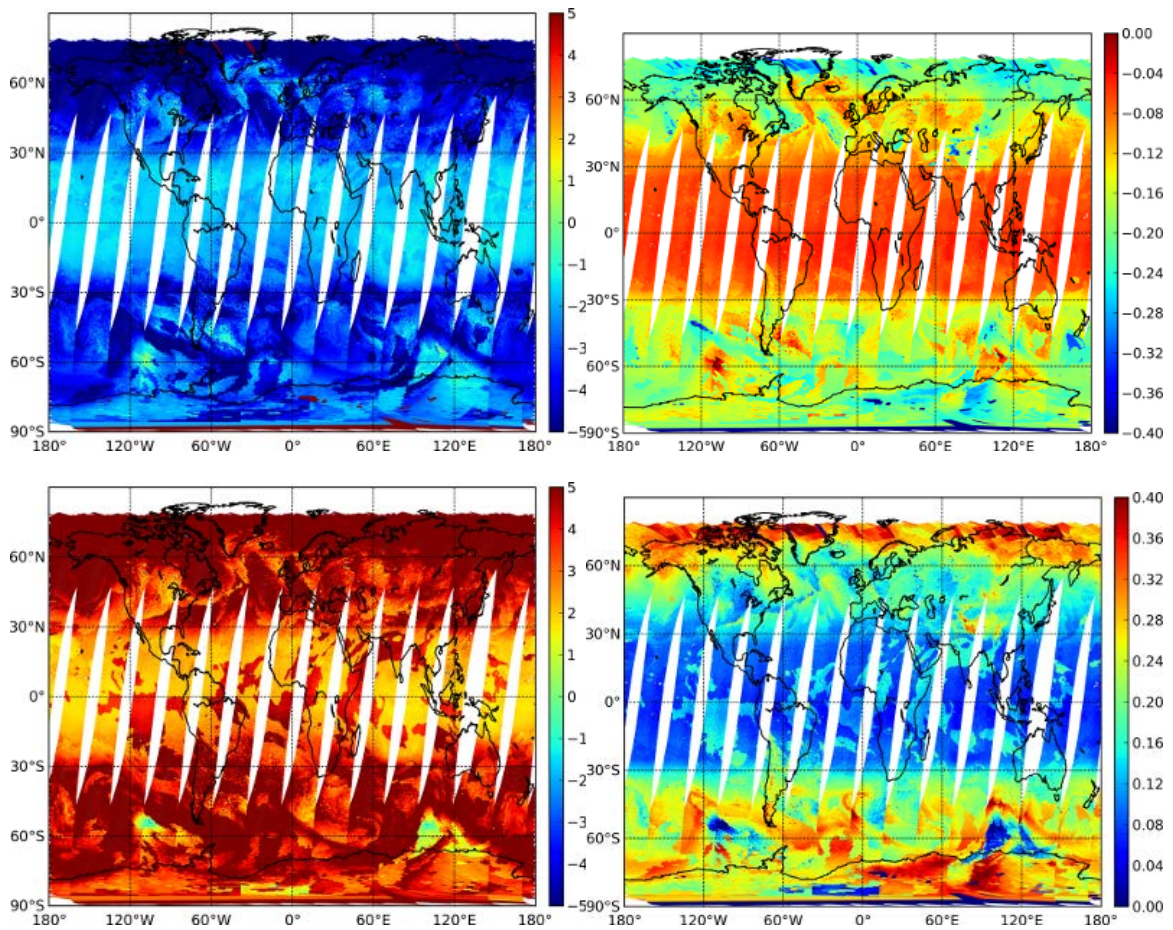


Figure 19: Top: absolute difference [in DU] between the standard TrOC versus using the tropopause level one layer lower (left) and its relative difference [as a fraction] (right). Bottom: the same for one level higher.

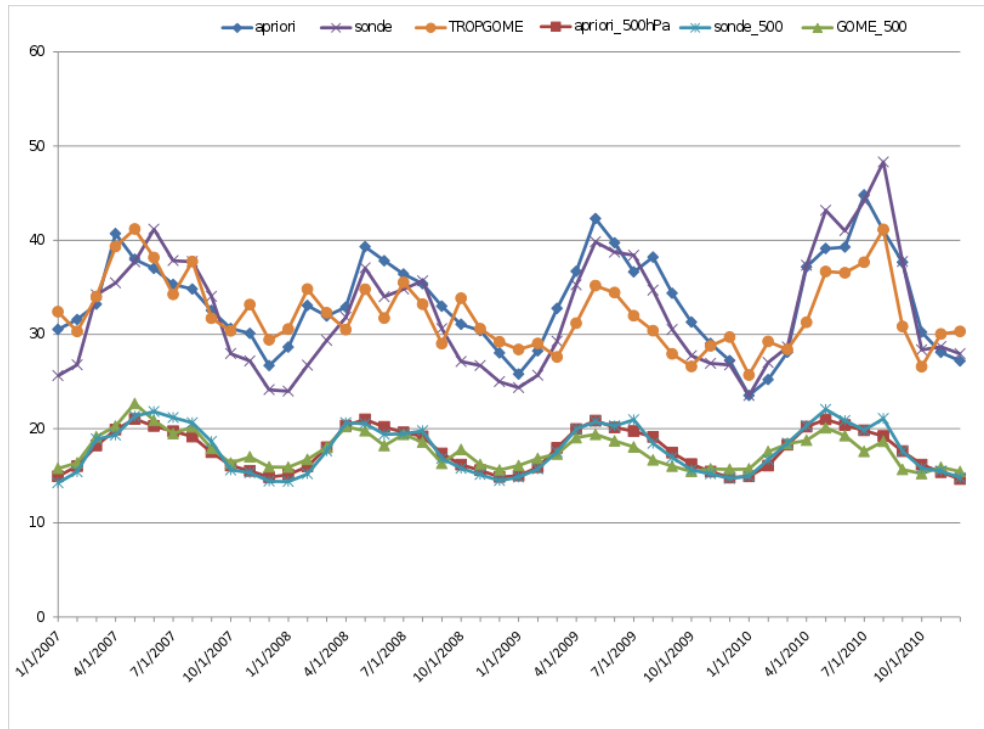


Figure 20: Tropospheric ozone column of modelled and observed tropospheric ozone columns (DU) (surface—T_{pl} and surface—500hPa) for reprocessed high resolution pixels for the station of Uccle.

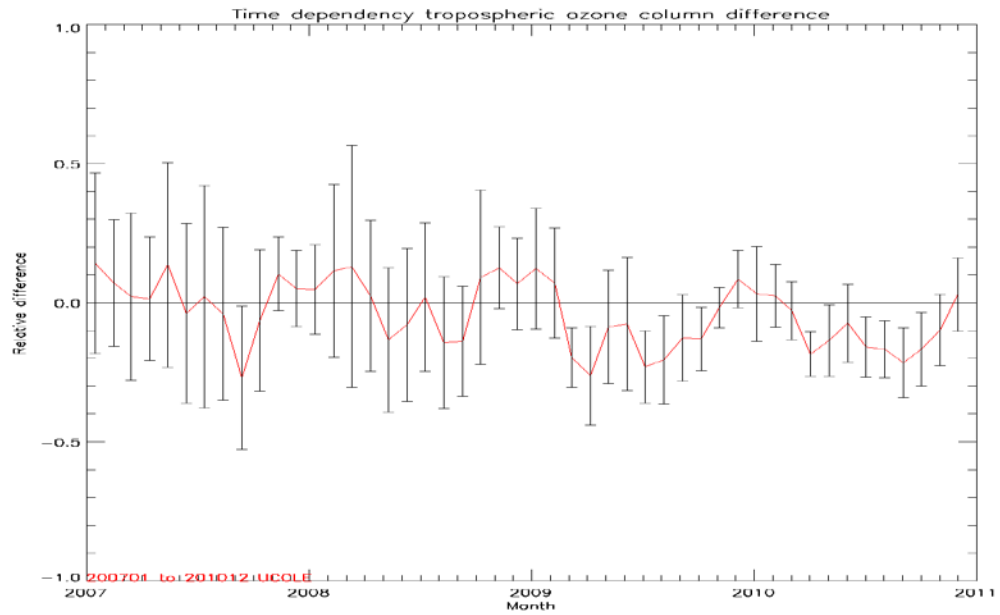


Figure 21: Relative difference between modelled and observed tropospheric ozone columns (%) for reprocessed high resolution pixels for the station of Uccle. The high resolution pixels show better results with a reduced standard deviation and less pronounced seasonal dependency. The average bias is -0.04 and the average stddev is 0.20 for the plot above.

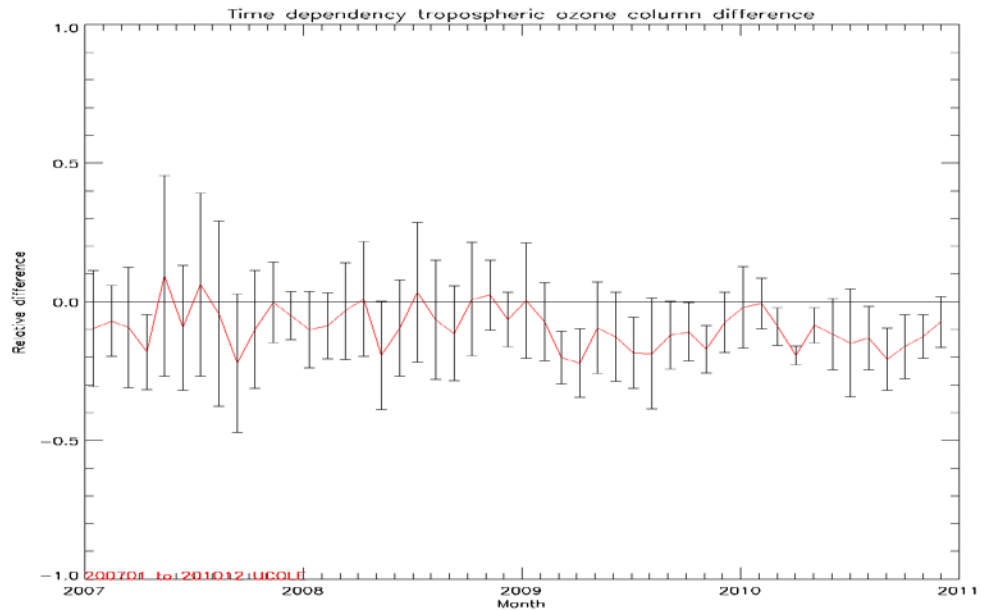


Figure 22: Relative difference between modelled and observed ozone columns from the surface to 500hPa (%) for reprocessed high resolution pixels for the station of Uccle. The average bias is lower than zero because Uccle has an over-estimation of ozone in its sonde retrievals near the surface. The seasonal dependence is no longer present compared to Figure 21 because the UTLS is not present (source: KMI).

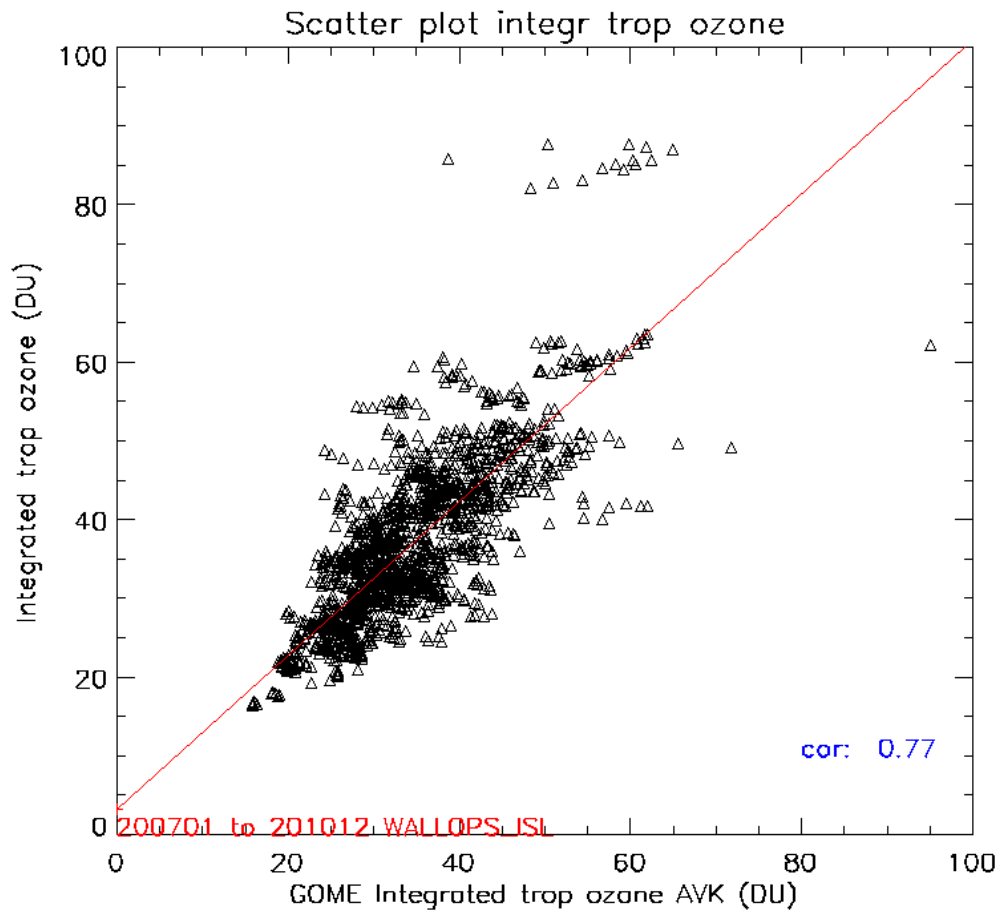


Figure 23: Scatter plot for integrated GOME-2 tropospheric ozone column data and the observed integrated tropospheric ozone column data, applying the averaging kernels, using coarse resolution pixels for the station of Wallops Island.

11. REFERENCES

- Anderson, G.P., S.A. Clough, F.X. Kneizys, J.H. Chetwynd, E.P. Shettle, *AFGL atmospheric constituent profiles*, 1986, in: Environmental research papers, no. 954, Air Force Geophysical Laboratory, AFGL-TR-86-0110
- Anderson, E., Z. Bai, C. Bischof et al., *LAPACK User's Guide*, Society for Industrial and Applied Mathematics, Philadelphia, 2nd edition, 1995
- Bass, A.M., R.J. Paur, *The UV cross-sections of ozone: 1. Measurements in atmospheric ozone.*, 1985, in: Proceedings of the quadrennial ozone symposium, p.606-616.
- Bates, D.R., *Rayleigh scattering by air*, Planet. Space Sci. 32, 785-790, 1984
- Berk, A., L. S. Bernstein, D. C. Robertson, *MODTRAN: A moderate resolution model for LOWTRAN-7*, GL-TR-89-0122, Geophysics Laboratory, Hanscom AFB, MA 01732, 1989.
- Bhartia, P.K., R.D. McPeters, C.L. Mateer, L.E. Flynn, C. Wellemeyer, *Algorithm for the estimation of vertical ozone profiles from the backscattered ultraviolet technique*, J. Geophys. Res 101, 18793-18806, 1996
- Brion, J., Chakir, A., Daumont, D., and Malicet, J.: High-resolution laboratory absorption cross section of O₃. Temperature effect, Chem. Phys. Lett., 213(5-6), 610-612, 1993.
- Burrows, J.P. et al. The Global Ozone Monitoring Experiment (GOME): mission concept and first scientific results, J. Atmos. Sci. 56, 151-175, 1999
- Chance, K.V, R.J.D. Spurr, *Ring effect studies: Rayleigh scattering, including molecular parameters for rotational Raman scattering and the Fraunhofer spectrum*, Applied Optics 36, 5224-5230, 1997
- Chance, K.V, J., P. Burrows, D. Perner, W. Schneider, "Satellite measurements of atmospheric ozone profiles, including tropospheric ozone, from ultraviolet/visible measurements in the nadir geometry: a potential method to retrieve tropospheric ozone", J. Quant. Spectrosc. Radiat. Transfer 57, 467-476, 1997
- Chance, K.V, *Wavelength calibration corrected Bass & Paur Ozone cross sections*, private communication, 2001
- Chandrasekhar, S., *Radiative Transfer*, Dover, New York, 1960
-

- Caudill, T.R., D.E. Flittner, B.M. Herman, O. Torres, R.D. McPeters, *Evaluation of the pseudo-spherical approximation for backscattered ultraviolet radiances and ozone retrieval*, J. Geophys. Res. 102, 3881-3890, 1997
- Daumont, M., Brion, J., Charbonnier, J., and Malicet, J.: Ozone UV spectroscopy I: Absorption cross-sections at room temperature, J. Atmos. Chem., 15, 145–155, 1992.
- Deepak, A. et al (ed), *Report of the Expert Meeting on Aerosols and Their Climate Effects*, World Climate Research Programme WCP-55, WMO, 1983.
- De Haan, J.F., P. Bosma, J. Hovenier, *The adding method for multiple scattering calculations of polarized light*, Astron. Astrophys. 181, 371-391, 1987
- De Haan, J.F., *Accounting for Raman Scattering in DOAS*, KNMI/OMI-technical document, SN-OMIE-KNMI-409, 2003
- De Haan, J.F., *private communication*, 2004
- DLR, GOME level 0 to 1 algorithms description, *Tech. Note ER-TN-DLR-GO-0022*, DLR/DFD, Oberpfaffenhofen, Germany, 1996. [DLR, 1996a]
- DLR, Product Specification Document of the GOME Data Processor ER-PS-DLR-GO-0016, Iss./Rev.3/C, 30/09/1996 [DLR, 1996b]
- DLR, GOME Data Processor Extraction Software User's Manual, ER-SUM-DLR-GO-0045, Issue 1, 4 August 1999
- Fortuin, J.P.F., U. Langematz, *An update on the global ozone climatology and on concurrent ozone and temperature trends*, in Atmospheric Sensing and Modelling, ed. R.P. Santer, Proc. SPIE 2311, 207-216, 1995
- Fortuin, J.P.F., H. Kelder, *An ozone climatology based on ozonsonde and satellite measurements*, J. Geophys. Res 103, 31709-31734, 1999
- Grainger, J.F., J. Ring, *Anomalous Fraunhofer line profiles*, Nature 193, 762, 1962
- Hasekamp, O., J. Landgraf, *Ozone profile retrieval from backscattered ultraviolet radiances: The inverse problem solved by regularization*, J. Geophys. Res., 106, 8077-8088, 2001
- Hasekamp, O.P., J. Landgraf, *A Linearized vector radiative transfer model for atmospheric trace gas retrieval*, J. Quant. Spectrosc. Radiat. Transfer, 75, 221-238, 2002
-

- Hasekamp, O.P., J. Landgraf and R.F. van Oss, *The need of polarization modelling for ozone profile retrieval from backscattered sunlight*. J. Geophys. Res., 107, 10.1029, 2002
- Herman, J.R., E.A. Celarier, *Earth surface reflectivity climatology at 340-380 nm from TOMS data*, J. Geophys. Res 102, 28003-28011, 1997
- Hoogen, R., V.V. Rozanov, J.P. Burrows, *Ozone profiles from GOME satellite data: Algorithm description and first validation*, J. Geophys. Res. 104, 8263-8280, 1999.
- Joiner, J., P.K. Bhartia, R.P. Cebula, E. Hilsenrath, R.D. McPeters, H. Park, *Rotational Raman scattering (Ring effect) in satellite backscatter ultraviolet measurements*, Applied Optics 34, 4513-4525, 1995.
- Kelder, H., et al. *European report on ozone-climate interactions*, 2003
- Koelemeijer, R.B.A. and P. Stammes, *A fast method for retrieval of cloud parameters using oxygen A-band measurements from the Global Ozone Monitoring Experiment*. J. Geophys. Res., 106, 3475-3490, 2001
- Koelemeijer, R.B.A., J.F. de Haan, and P. Stammes, *A database of spectral surface reflectivity in the range 335-772 nm derived from 5.5 years of GOME observations*, J. of Geophys. Res., 108, 4070, 2003.
- Lacis, A.A., J. Crowdry, M. I. Mischenko, B. Cairns, *Modeling errors in diffuse sky radiation: Vector vs. scalar treatment*, Geophys. Res. Lett. 25, 135-138, 1998
- Landgraf, J., O. Hasekamp, M. Box, T. Trautmann, *A Linearized Radiative Transfer Model for Ozone Profile Retrieval Using the Analytical Forward-Adjoint Perturbation Theory Approach*, J. Geophys. Res., 106, 27,291-27,305, 2001
- Liou, K. N., *Analytic two-stream and four-stream solutions for radiate transfer*, J. Atmos. Sci. 31, 1473-1475, 1974
- Malicet, C., Daumont, D., Charbonnier, J., Parisse, C., Chakir, A., and Brion, J.: *Ozone UV spectroscopy, II. Absorption cross-sections and temperature dependence*, J. Atmos. Chem., 5 21, 263–273, 1995.
- McPeters R.D., Labow G.J., Logan J.A. : *Ozone climatological Profiles for Satellite Retrieval Algorithms*, J. Geophys. Res., vol 112, D05308, 2007.
- Meijer Y. J., et al. (2006), *Evaluation of Global Ozone Monitoring Experiment (GOME) ozone profiles from nine different algorithms*, J. Geophys. Res., 111, D21306, doi:10.1029/2005JD006778.
-

- Mischenko, M.I., A. A. Lacis, L. D. Travis, *Errors induced by the neglect of polarization in radiance calculations for Rayleigh-scattering atmospheres*, J. Quant. Spectrosc. Radiat. Transfer 51, 491-510, 1994
- Müller, M. D., A. K. Kaifel, M. Weber, S. Tellmann, J. P. Burrows, and D. Loyolla, *Ozone profile retrieval from GOME data using a neural network approach (NNORSY)*, J. Geophys. Res., accepted for publication, 2003
- Munro, R., Siddans, R., Reburn, W.J., Kerridge, B.J., *Direct measurement of tropospheric ozone distributions from space*, Nature 392, 168-171, 1998
- Nakajima, T., M. Tanaka, *Algorithms for radiative intensity calculations in moderately thick atmospheres using a truncation approximation*, J. Quant. Spectrosc. Radiat. Transfer 40, 51-69, 1988
- Orphal, J, *A Critical Review of the Absorption Cross-sections of O₃ and NO₂ in the 240-790 nm Region. Part 1. Ozone*. ESA Technical Note MO-TN-ESA-GO-0302, 126 pp., 2002
- Rodgers, C.D., *Retrieval of atmospheric temperature and composition from remote measurements of thermal radiation*, Rev.Geoph.Sp.Phys. 14, 609-624, 1976
- Rodgers, C.D., *Characterisation and error analysis of profiles retrieved from remote sounding experiments*, J. Geophys. Res 95, 5587-5595, 1990
- Rodgers, C.D., *Inverse methods for atmospheric sounding*, World Scientific Publishing Pte Ltd, New York, 2000
- Rothman, L.S., et al., *The HITRAN molecular database: Editions of 1991 and 1992*, J. Quant. Spectrosc. Radiat. Transfer 48, 469-507, 1992
- Rozanov, V.V., T. Kurosu, J.P. Burrows, *Retrieval of atmospheric constituents in the UV-visible: A new quasi-analytical approach for the calculation of weighting functions*, J. Quant. Spectrosc. Radiat. Transfer 60, 277-299, 1998
- Rozanov, A.V., V.V. Rozanov, J.P. Burrows, *Combined differential-integral approach for the radiation field computation in a spherical shell atmosphere: Nonlimb geometri*”, J. Geophys. Res. 105, 22937-22942, 2000
- Schutgens, N.A.J. and Stammes, P.: 2003, *A novel approach to the polarisation correction of space-born spectrometers*, J. Geophys. Res. 108 (D7), doi 10.1029/2002JD002736.
- Singer, S.F., R.C. Wentworth, *A method for the determination of the vertical ozone distribution from a satellite*, J. Geophys. Res. 62, 299-2308, 1957
-

- Spurr, R.J.D., *Linearized Radiative Transfer Theory*, Proefschrift Technische Universiteit Eindhoven, 2001
- Spurr, R.J.D., T.P. Kurosu, K.V. Chance, *A linearised discrete ordinate radiative transfer model for atmospheric remote sensing retrieval*, J. Quant. Spectrosc. Radiat. Transfer 68, 689-735, 2001
- Spurr, R.J.D. *Simultaneous radiative transfer derivation of intensities and weighting functions in a general pseudo-spherical treatment*, J. Quant. Spectrosc. Radiat. Transfer, 75, 129–175, 2002
- Spurr, R.J.D. *Discrete Ordinate Theory in a Stratified Medium with First Order Rotational Raman Scattering; a General Quasi-Analytic Solution*, in preparation, 2003
- Stammes, P., *Errors in UV reflectivity and albedo calculations due to neglecting polarisation*, Proc. of SPIE, Atmospheric Sensing and Modelling, Vol. 2311, p.227-235, 1994
- Stamnes, K, S.-C. Tsay, W. Wiscombe, K. Jayaweera, *Numerically stable algorithm for discrete-ordinate-method radiative transfer in multiple scattering and emitting layered media*, Applied Optics 27, 2502-2509, 1988
- Twomey, S., *On the deduction of the vertical distribution of ozone by ultraviolet spectral measurements from a satellite*, J. Geophys. Res. 66, 2153-2162, 1961
- Vandaele, A.C., C. Hermans, P.C. Simon et al., *Measurements of the NO₂ absorption cross-sections from 42,000 cm⁻¹ to 10,000 cm⁻¹ (238-1000nm) at 220K and 294K*, J. Quant. Spectrosc. Radiat. Transfer 59, 171-184, 1998
- Van Geffen, J.H.G.M., Documentation of the software package GomeCal (version 1.0), Technical report, KNMI, De Bilt, The Netherlands, TR-255, 2002
- Van Geffen, J.H.G.M. and R.F. Van Oss, *Wavelength calibration of spectra measured by GOME using a high-resolution reference spectrum*, Applied Optics, 42, 2739-2753, 2003
- Van der A, R.J., R.F. van Oss, H. Kelder, *Ozone profile retrieval from GOME data*, in Satellite Remote Sensing of Clouds and the Atmosphere III, Jaqueline E. Russel, Editor, Proceedings of SPIE Vol. 3495, 221-229, 1998
- Van der A, R.J., R.F. van Oss, A.J.M. Piters, J.P.F. Fortuin, Y.J. Meijer and H. Kelder. *Ozone profile retrieval from recalibrated Global Ozone Monitoring Experiment data*. J. Geophys. Res. 107, 10.1029, 2002
-

- Van der A, R.J., Van Oss, R.F., Peters, A.J.M., Fortuin, J.P.F., Meijer, Y.J. and Kelder H.M.: 2002, *Ozone profile retrieval from recalibrated Global Ozone Monitoring Experiment data*, J. Geophys. Res. 107, 10.1029.2001JD000696.
- Van Oss, R.F., R.J.D. Spurr, *Fast and accurate ozone profile retrieval for GOME and GOME-2*, Proc. ERS/ENVISAT Symposium 2000, Gothenburg, ESA, 2000
- Van Oss, R., R.J.D. Spurr, *Fast and accurate 4 and 6 stream linearised discrete ordinate radiative transfer models for ozone profile remote sensing retrieval*, J. Quant. Spectrosc. Radiat. Transfer, 75, 177-220, 2002
- Van Roozendaal, M., in: Lambert, J.C. (ed), ERS-2 GOME GDP 3.0 Implementation and Delta Validation. Validation Report for GOME Level-1-to-2 Data Processor Upgrade to Version 3.0, ERSE-DTEX OAD-TN-02-0006, Version 1.0, November 2002
- Voors, R., Dirksen, R., Dobber, M., Levelt, P., "OMI In-Flight Wavelength Calibration and the Solar Reference Spectrum", Atmospheric Science Conference, 2006, ESA Special Publication, Vol. 628.
- Vountas, M., V.V. Rozanov, J.P. Burrows, *Ring effect: impact of rotational Raman scattering on radiative transfer in Earth's atmosphere*, J. Quant. Spectrosc. Radiat. Transfer 60, 63-77, 1998
- Wang, P., Stammes, P., "FRESCO-GOME2 project, Additions to EPS/MetOp RAO project #3060, EUM/CO/06/1536/FM, WP1: FRESCO algorithm and database updates", KNMI, 2007
- Wiscombe, W.J., The delta-M method: rapid yet accurate radiative flux calculations for strongly asymmetric phase functions, J. Atmos. Sci. 34, 1408-1422, 1977.
- WMO, Manual on Codes, International Codes, VOLUME I.1, Part A — Alphanumeric Codes, WMO–No. 306, (1995 edition)
- Zehner, C., *New Total Ozone Retrieval Algorithm Using GOME Measurements (TIDAS/SAMF)*, PhD Thesis at Karl Franzens University Graz, 2005.
-